ATMOSPHERIC KINETIC ENERGY AT 500 MB

ATMOSPHERIC KINETIC ENERGY AT 500 MB AS A FUNCTION OF ZONAL WAVE NUMBER

by

F.M. Luistro

A thesis submitted to the Faculty of Graduate Studies and Research in partial fulfilment of the requirements for the degree of Master of Science.

Department of Meteorology,
McGill University,
Montreal.

January, 1965

PREFACE

An adequate portrayal of the global distribution of kinetic energy is fundamental to our understanding of the general circulation of the atmosphere.

Since there are insufficient wind observations to carry out direct computations it is customary to supplement them with pressure or geopotential height data and to use space and time continuity to obtain analyzed weather maps. The geostrophic wind formula then permits one to recover kinetic energy to a good approximation, except in equatorial regions. This study is based on weather maps, for the International Geophysical Year, provided by official Weather Services. The accuracy of such charts is clearly relevant but was beyond the scope of this project.

In its dynamical research, McGill's Department of Meteorology makes wide use of analyzed weather maps and of zonal harmonic analysis to represent their derived fields. In this study, these investigations have been extended to cover the extra-equatorial regions of both hemispheres, for the first time.

TABLE OF CONTENTS

Table of Contents (continued)

LIST OF FIGURES

Figure		Page

LIST OF TABLES (APPENDIX)

ABSTRACT

Atmospheric kinetic energy computations at 500 mb are done for both hemispheres, excepting the tropical zone (20S to 20N), on a daily basis during September 1-30, 1957, one full month of the International Geophysical Year. The basic computational elements are the geopotential-height grid point values taken at every five degrees of latitude and at every ten degrees of longitude. Fourier analysis techniques are employed to determine the kinetic energy spectra as a function of zonal wave numbers.

Comparative analysis of the energy profiles of the two hemispheres shows that (i) the total kinetic energy is greater in the southern hemisphere; (ii) the zonal flow energy of the southern hemisphere is roughly three times that of the northern hemisphere, while their mean perturbation energies are approximately of the same magnitude; and (iii) the mean zonal energy is greater than the mean perturbation energy in the southern hemisphere and vice versa in the northern hemisphere.

INTRODUCTION

The Problem

While the common man stands in awe at the nature and complexity of the atmosphere, the meteorologist turns a searching mind toward the cause and effect of its physical phenomena. The complex energetics that propel the winds often befuddle him, but the maintenance of such seemingly endless air motions continually sparks his imagination.

This state of affairs has inspired the atmospheric scientists of the last decade or so to pursue their investigations of the enveloping atmosphere of our planet.

One paramount aspect of these extensive studies is the investigation of energy of the atmosphere. Others have done studies on scales, limited either in time or in space; but no one has done a thorough probe of the kinetic energy spectra in a broad space and time coverage. The writer did not intend to undertake such a herculean task of energy computations; however, he did carry out an initial phase by working on a mid-tropospheric standard pressure level, 500 mb, for a full month (September, 1957) of the International Geophysical Year for both hemispheres from their respective poles down to 20 degrees latitude.

Data Sources

Past theoretical investigations of atmospheric kinetic energy have been limited to restricted sectors for a specified time period, in spite of the availability of sophisticated mathematical methods for hemispheric analysis and high-speed computers to handle monumental data computations, because the inadequacy of data (more specifically, upper air data) was appalling enough to discourage a global study of any general circulation parameter.

In order to fill this big gap the International Geophysical Year was launched. One of the salient objectives of this international project

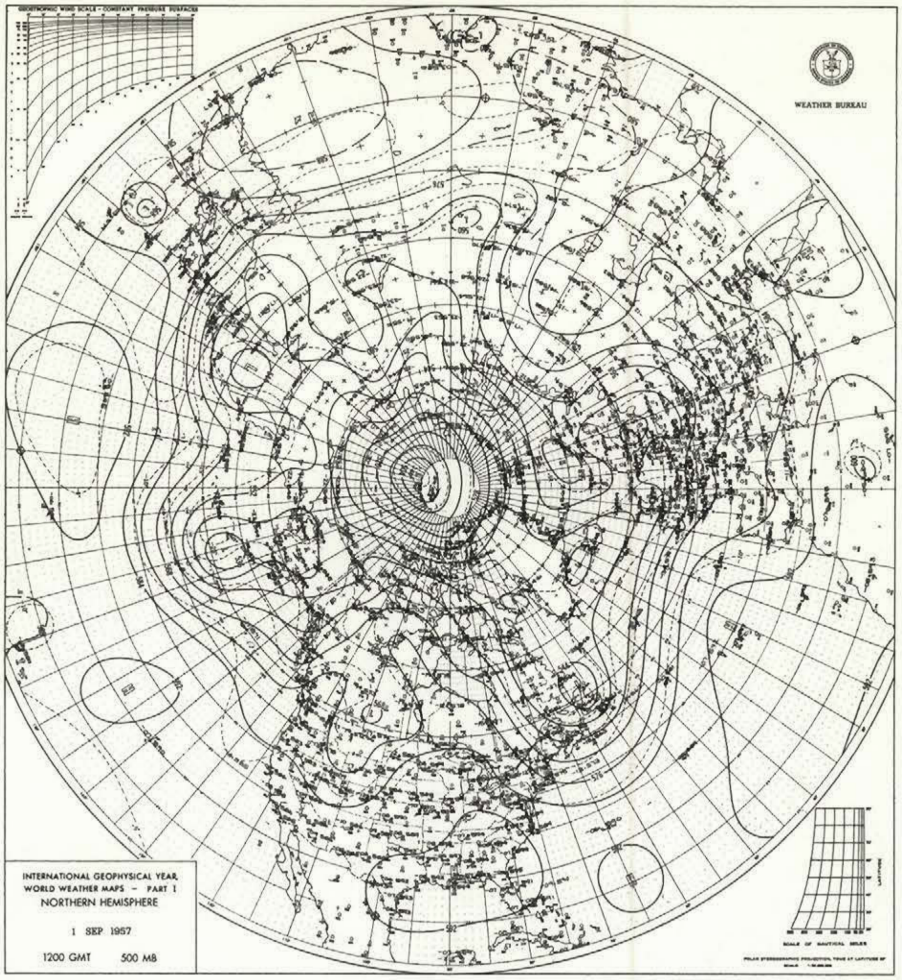

SEPTEMBER 1957

International Geophysical Year

WORLD WEATHER MAPS

Part I

Northern Hemisphere

Sea Level and 500 Millibar Charts

SEPTEMBER 1957

FIG. 1

was to provide a vast network of new observation stations in far-flung corners of the globe and to increase the frequency of observations at the existing ones. For the first time, continuous data were reported from the geographic poles.

An I. G. Y. Special Committee decided that world daily weather maps were to be prepared and published at a later date. Three nations - Federal Republic of Germany, Republic of South Africa, and the United States of America - divided the assignment to facilitate the task; U.S.A, to handle Part I (Northern Hemisphere, 20N to the pole), F.R.G., Part II (25S to 25N), and R.S.A., Part III (Southern Hemisphere, 20S to the pole).

The I. G. Y. World Weather Maps consist of a daily series of maps for the period July 1, 1957 to December 31, 1958. These maps are published as monthly booklets, each containing a surface and 500 mb map for 1200 GMT each day. Each hemispheric chart (Parts I and III) is a polar stereographic projection from 20 degrees latitude to the pole with the true scale of 1 to 50 million at latitude sixty degrees.

The writer chose the month of September, 1957 as his source data period upon the suggestion of his research supervisor, Professor B. W. Boville, as part of a future plan to correlate the energy profiles to typhoon and hurricane activity in the northern hemisphere. September is the month when intense cyclones accompanied by strong winds and heavy precipitation are prevalent in the tropics and subtropical belts.

Figures 1 and 2 show typical I. G. Y. World Weather Maps where the isolines are the geopotential height contours drawn on a 500 mb pressure surface. The 500 mb surface was chosen because it is in the middle of the troposphere by height considerations, and it is also in the middle of the whole atmosphere as far as mass is concerned.

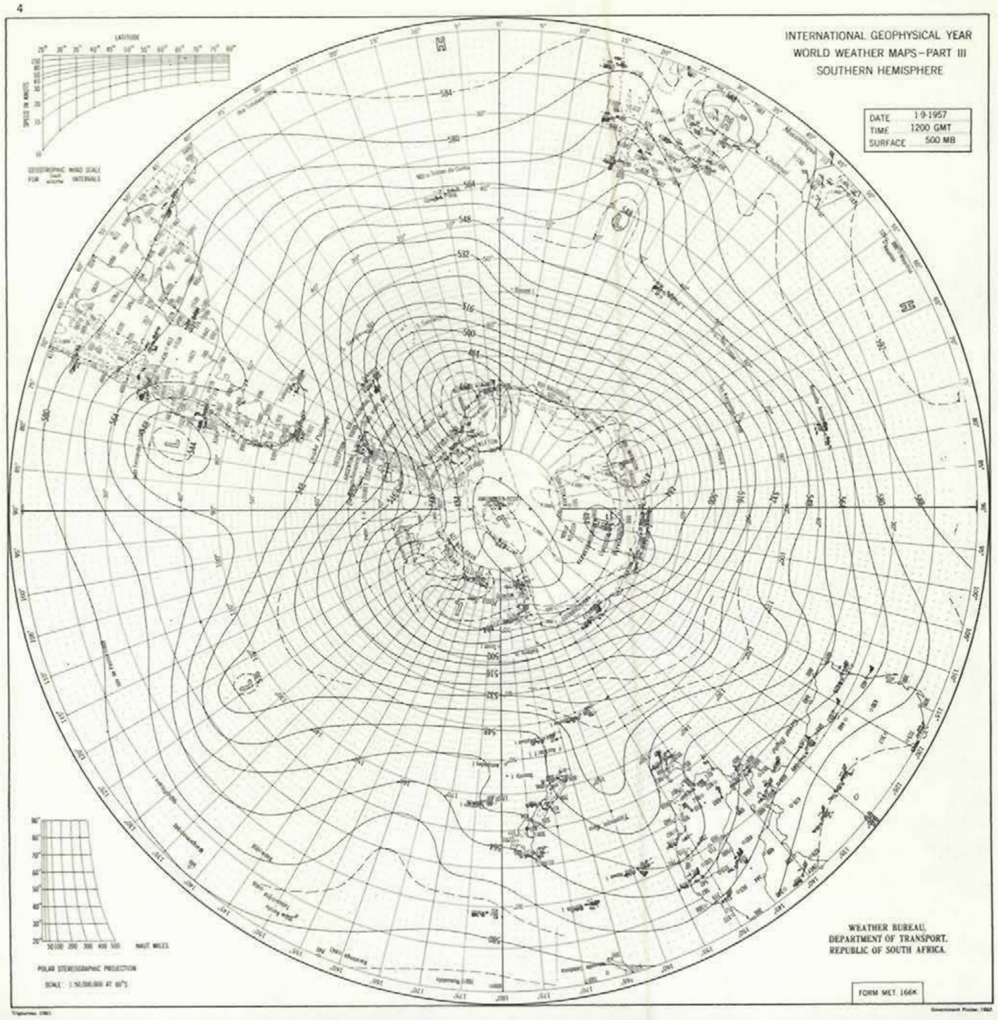
4
INTERNATIONAL GEOPHYSICAL YEAR
WORLD WEATHER MAPS—PART III
SOUTHERN HEMISPHERE
DATE 1-9-1957
TIME 1200 GMT
SURFACE 500 MB
GEOSTROPHIC WIND SCALE
POLAR STEREOGRAPHIC PROJECTION
WEATHER BUREAU,
DEPARTMENT OF TRANSPORT,
REPUBLIC OF SOUTH AFRICA.
FORM MET. 166K

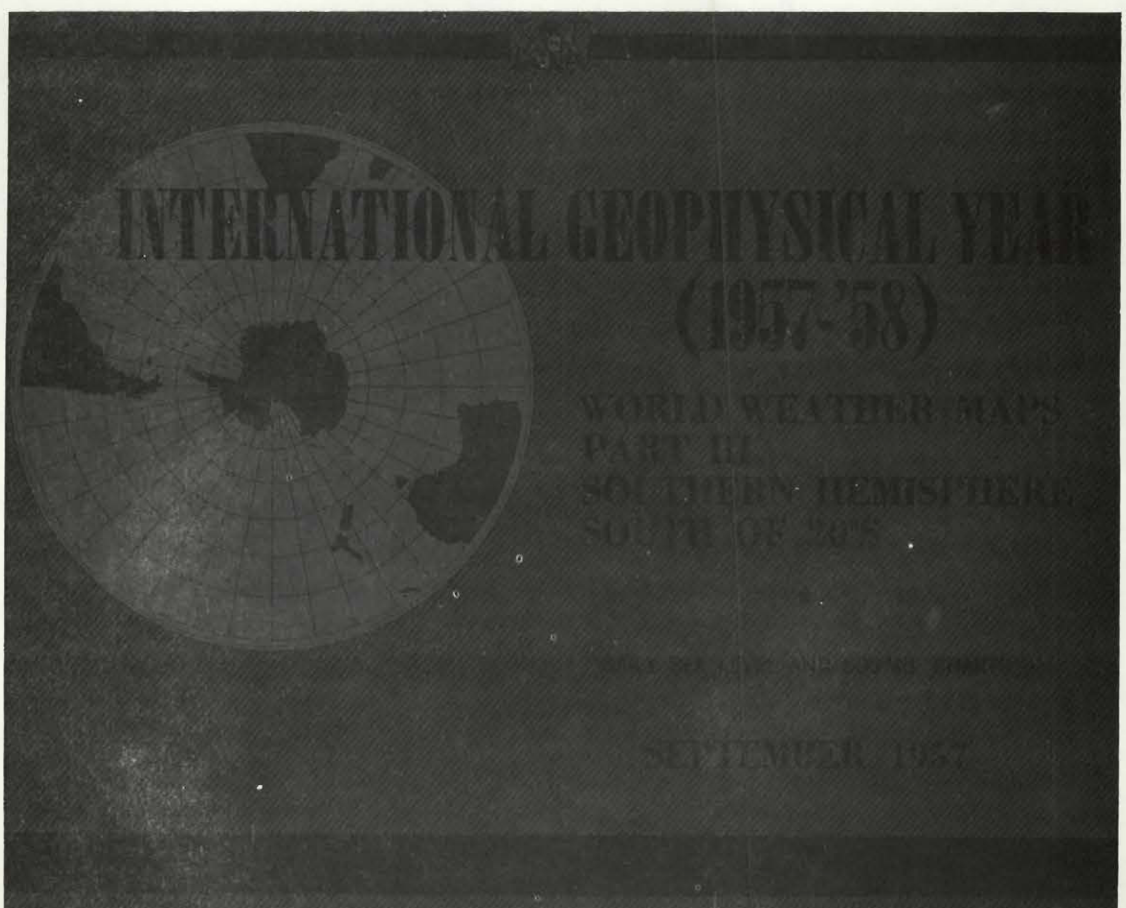
INTERNATIONAL GEOPHYSICAL YEAR
(1957-'58)
WORLD WEATHER MAPS
SOUTHERN HEMISPHERE

FIG. 2

Data Verification

The voluminous amount of data extraction was anticipated so that timely assistance was amply provided in this particular task by B. Cabacungan and J. de las Alas, co-employees of the writer in the Philippine Weather Bureau and currently taking graduate work at McGill University. All in all, 60,480 grid point data were extracted and punched on 5,040 IBM computer cards.

In the initial stages of the task, it was foreseen that in data extraction of this magnitude, commission of errors would be inevitable. To eliminate these errors entirely; or at least, to cut down the number to a negligible amount, a system was arranged in which two complete sets of data would be extracted from the same map, independently, by two different persons.

It did not take long for the writer to realize that this enormous bulk of punched data could bring about serious problems in verification. Three distinct and thorough methods of checking were carried out successively to filter out a different type of error in each process. These are enumerated hereunder:

(i) IBM Sorting Machine Method - The automatic sorter-counter conveniently showed the discrepancies in the number of cards for each day, for each latitude, and for each hemisphere. Likewise, errors in the sequences of cards were noted and rectified. The sorter was also operated to detect double punch errors. This type of error proved to be a real nuisance because the computer would not operate when a double punch error was encountered because the program was designed for numerical format and not for alphabetic format where double punches are used.

(ii) Print-out Data Method - It became apparent that mere machine counting and correct sequences of cards were not sufficient enough to guarantee flawless input. For example, the number of cards could be correct but a duplication could easily cover up an omission.

As a last resort to eradicate these mechanical errors, all the data were printed out from the computer. Errors, like omission and duplication of data, wrong alignment and order of data were visually spotted and corrected.

(iii) Machine Programming Method - After all the mechanical errors were eliminated, the next phase of verification was to test the reliability and accuracy of the data extracted. As was mentioned before, two sets of similar data were independently extracted by two different individuals.

A computer program was written to compare the two similar but independent data within a tolerance of plus-and-minus one (actually equal to ten meters, the unit used in data extraction). Errors caused by misreading, wrong interpolation and extrapolation, wrong subjective interpretation, wrong maps used, and individual differences were cleared through this last step of verification.

This scheme of three successive separate methods of verification proved to be very effective in reducing the errors practically to nil.

Another help in the verification process was the occasional appearance of glaring errors in the printed outputs in the form of disproportionate values of variables (amplitudes, energy amounts, etc.) particularly in the higher wave numbers of the spectra. A few final errors that escaped detection in the rigorous methods of verification were noticed in this manner - apparently spurious outputs were easily distinguished from expected values.

The Fourier Analysis Technique

It is common meteorological knowledge that the atmospheric motion systems tend to lie along latitude circles distributed around the earth and be wave-like in character. This justifies the extensive use of zonal harmonic analysis in general circulation studies.

The most popular and convenient of these analytic methods is Fourier series analysis. "Fourier analysis appears as a natural method for distinguishing different scales of disturbances embedded in a mean flow. From a mathematical viewpoint such a resolution seems very practical and desirable since the orthogonality property of sinusoidal functions permits one to write energy equations for these separate components in a relatively straightforward fashion." (Boville, Kwizak, 1959).

However, Fourier representation of meteorological parameters in global circulations is only applicable and practical where there are adequate data coverage and modern computation facilities.

Expanding in Fourier series an arbitrary meteorological parameter associated with the atmospheric motion systems (such as Z-, the geopotential height of a constant pressure surface), function of longitude λ, along a latitude circle ϕ, at pressure level p, and time t, we obtain the classical formulae:

$$Z_\lambda = A_o(\phi) + \sum_n A_n(\phi) \cos n\lambda + \sum_n B_n(\phi) \sin n\lambda \quad \ldots(1)$$

where:

$$A_n(\phi) = \frac{1}{\pi} \int_o^{2\pi} Z_\lambda \cos n\lambda \, d\lambda = \frac{2}{N} \sum_{N=1}^{N} Z_N \cos n\lambda_N$$

$$A_o(\phi) = \frac{1}{2\pi} \int_o^{2\pi} Z_\lambda \, d\lambda = \frac{1}{N} \sum_{N=1}^{N} Z_N$$

$$B_n(\phi) = \frac{1}{\pi} \int_o^{2\pi} Z_\lambda \sin n\lambda \, d\lambda = \frac{2}{N} \sum_{N=1}^{N} Z_N \sin n\lambda_N$$

N is the number of grid points around a latitude circle.

Note: n - the zonal wave number, represents the number of equally spaced waves (troughs/ridges) around a latitude circle.

Thus, Z, at any longitude, λ, is decomposed into a mean height, A_o, and contributions from a series of sine and cosine waves.

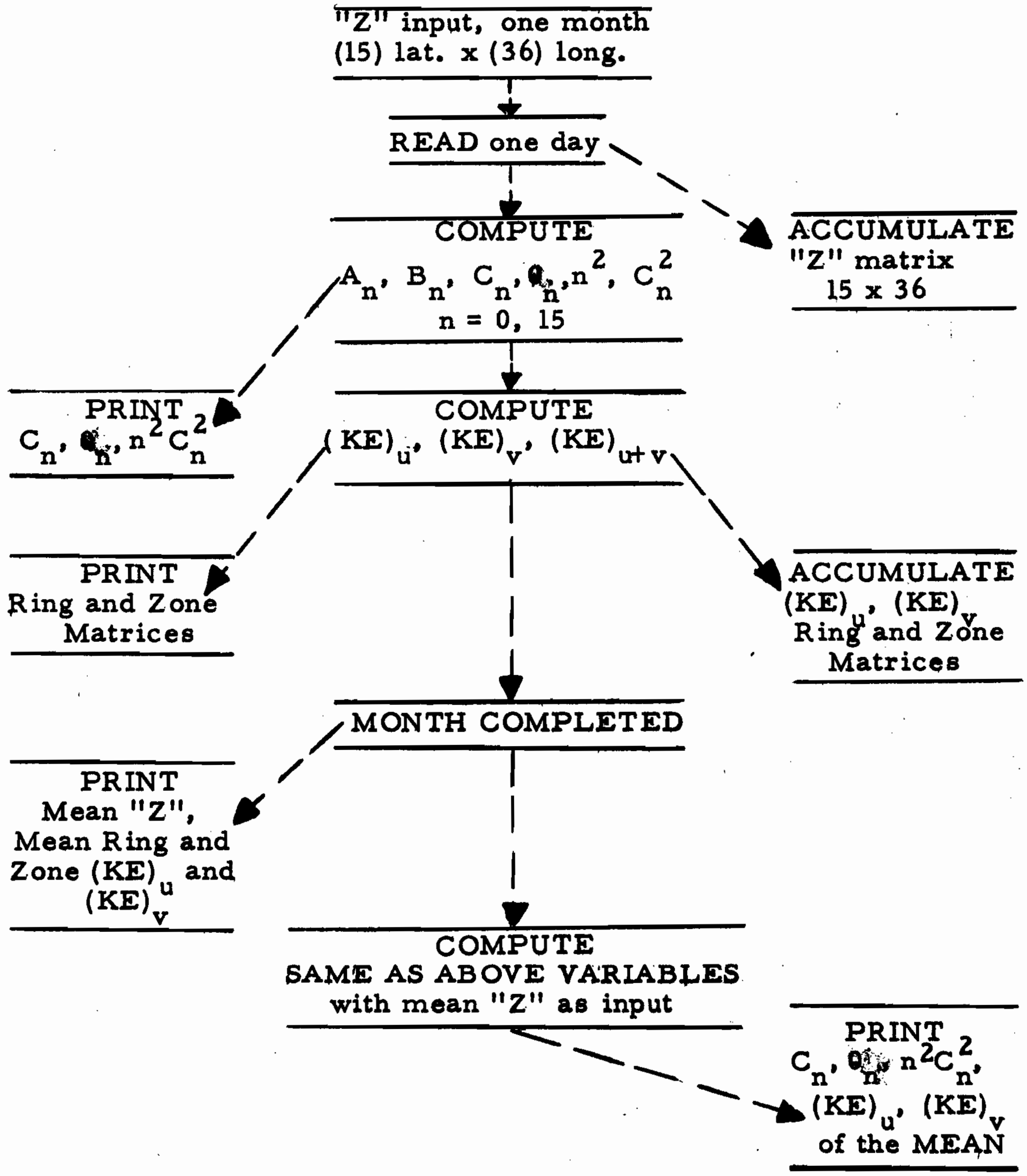

Figure 3. Schematic flow chart showing the input, storage, and output.

This Fourier notation of $\underline{Z}$ can also be represented as

$$Z = A_o + \sum_n C_n(\phi) \cos\left[n\lambda - \theta_n(\phi)\right] \qquad \ldots(2)$$

where $C_n(\phi)$, the amplitude of wave $\underline{n}$ is defined by

$$C_n(\phi) = (A_n^2(\phi) + B_n^2(\phi))^{1/2}$$

and $\theta_n(\phi)$, the phase angle of wave $\underline{n}$, is defined by

$$\theta_n(\phi) = \arctan(B_n/A_n).$$

Data Processing

The application of Fourier series analysis to any set of data implies in most cases the existence of uniform grid points on source synoptic charts (usually circumpolar maps) from which data are extracted. The grid used here consisted of 36 points at ten-degree intervals (originating from the Greenwich meridian going east) around each latitude circle. The latitude circles were five degrees apart, starting from 20 degrees to the poles, each hemisphere giving a total of fifteen. While this type of grid has the disadvantage of unequal area sampling due to the converging of meridians at the poles; it has, nevertheless, been adopted for convenience in data reading and computations.

Geopotential heights in tens of meters were extracted from the 500 mb I. G. Y. circumpolar charts for each of the project days (September 1-30, 1957).

The cards were processed through McGill's IBM 7040, 32,000-word digital computer. The output for each latitude, each day, the accumulated matrices and the print-out data are best described and illustrated in Figure 3 showing the schematic general flow of the programmed phase of the task.

SOME ASPECTS OF PAST ATMOSPHERIC KINETIC ENERGY INVESTIGATIONS

One of the essential meteorological parameters in general circulation studies is the kinetic energy of atmospheric zonal winds and of the eddies or perturbations embedded in the mean zonal flow.

Along with angular momentum and heat transport, kinetic energy has always been the object of discussion and investigation among the researchers in general circulation.

In this section, the writer will not refer to studies concerning transfers and conversions of the different forms of energy, energy budget, and energy interactions between vertical layers or between latitudinal belts, as he will not deal with them in this paper. Rather, he will touch on the energy spectra research conducted in the light of new developments in the theories of dynamical meteorology aided by modern mathematical tools and models of the atmosphere.

So far the energy wave spectrum has been probed only for relatively brief periods, specific latitude sectors, and for selected constant pressure surfaces.

Van Mieghem, Defrise, and Van Isacker (1960) studied the kinetic energy at 50-55N for two winter periods (Nov. 1, 1950 - Feb. 28, 1951, and Jan. 1, 1953 - April 30, 1953) at 500 mb surface and emerged with the following results:

(i) The kinetic energy of the disturbed westerlies was distributed between both moving waves and quasi-stationary waves (the latter being identified by the use of 10-day running mean charts which suppressed the moving systems). The quasi-stationary waves had a sharp peak at wave number 3, with negligible amounts beyond 4. Numbers 1 and 2 (eccentricity and bipolarity) also contributed significant amounts.

(ii) The moving waves had roughly similar amounts of energy at all wave numbers from 1 to 10, and comprised two sub-classes: the long moving waves, in jet-stream surges, that affected the zonal motion, and the cyclone waves (5 or 6 and up), which had most effect on the meridional motion.

Boville (1961) and his associates at McGill University in a similar investigation used Fourier components of the 25 mb height profile along latitude circles at 5 degree intervals from 40N to 80N for every fifth day. Later, Boville elaborated on this in a separate study by extending his analysis vertically and chose the winter of 1958-1959 for his source period. His summarised results regarding kinetic energy are as follows: over the 40-80N zone, most of the eddy kinetic energy at 25 mb and 100 mb (approximately 24 and 15 km in these latitudes) was in the long waves over this winter period, the maximum being at n=2 at 100 mb and n=1 at 25 mb. At the higher level half the total kinetic energy was in the eddies and half in the zonal flow, with negligible amounts beyond n=5. By contrast, at 500 mb two thirds of the energy was in the eddies, with a peak at n=3, but with a wide and roughly uniform distribution over wave numbers 1 to 5, and with considerable amounts out to n=8.

Robert M. White and Duane S. Cooley (1956) of Air Force Cambridge Research Center made a study of the daily kinetic energy spectra of meridional motions at 500 mb at latitude 45N for a 3-month winter period (Dec., 1949 - Feb., 1950). A pron ounced characteristic of the resulting spectra is the occurrence of a double maximum, indicating the existence of two distinct wave-number bands in the mid-troposphere. These two wave-number bands are centered around wave numbers 4 and 8.

Charney(1951) of the Massachusetts Institute of Technology likewise produced a mean spectral distribution of the kinetic energy of north-south motions for 500 mb at 45N for a three-day period (Jan.

11-13, 1949). He obtained two distinct energy maxima also, but at wave numbers averaging 2.5 and 7.5 with a minimum at wave number 4. The discrepancy (as compared with White and Cooley) in the low end of spectrum may be due to the fact that Charney's data were based on only three days of observation.

S. Kubota and M. Iida (1956)* of Tokyo University, who performed harmonic analysis at the 500 mb level, at the latitude circles 30, 45, and 50N, for the periods January, 1949 and May-July, 1951, showed marked seasonal displacements of the troughs and ridges of wave numbers 1 and 2 (except at 30N), and very small changes with season in the positions of the troughs and ridges of wave number three.

Saltzman (1958), who worked on the means of daily kinetic energy spectra for January 1949 for three latitudes, revealed that the profiles show a tendency for the variations of the zonal wind around a latitude circle to be of larger wave length than the variations of the meridional velocity component. In particular, wave numbers 1 to 3 in the zonal kinetic energy are dominant at all three latitudes. He observed that the greatest spread of energy over the various wave numbers occurs at 47.5N. This result is not surprising in view of the fact that the mid-latitudes are the seat of the transient cyclones which display great variations in size and intensity depending on the stage of development. The low and high latitudes (27.5N and 67.5N) in his investigation on the other hand are generally the locations of the more regular 'semi-permanent' centers. In the zonal kinetic energy spectra there is a striking occurrence of energy in wave number one which indicates that the zonal current tends to be more intense on one side of the hemisphere than the other.

Wiin Nielsen (1959) concentrated on energy conversion computations for different wave numbers for the months of January and April 1959. It was found that an adiabatic frictionless computation showed 2 maxima for the wave lengths corresponding to 2 and 6 or 7 waves around the hemisphere. He showed that the maximum which

* after Van Mieghem

appears for the very long waves most likely would disappear if heat sources and sinks could be taken into account. It seems therefore the very long waves will receive the main part of the kinetic energy through a non-linear interaction with the shorter waves.

Obasi (1963) under Starr at the M. I. T. Planetary Circulations Project worked extensively on energy calculations for the southern hemisphere during the International Geophysical Year. He showed the overwhelming importance of the transient eddies as the major sources of the kinetic energy of the mean zonal flow and the apparent inefficiency of the mean meridional motion in maintaining the mean zonal flow against frictional dissipation.

KINETIC ENERGY CALCULATIONS

Kinetic Energy Basic Equations

The equation of motion in the atmosphere in its vector form can be expressed as

$$\frac{d\mathbf{V}}{dt} = -\alpha\nabla P - 2\mathbf{\Omega} \times \mathbf{V} + \mathbf{g} + \mathbf{F} \qquad \ldots(3)$$

If this is multiplied scalarly by the velocity $\underline{V}$, we obtain

$$\frac{d}{dt}\left(\frac{V^2}{2} + gz\right) = -\alpha\mathbf{V}\cdot\nabla P + \mathbf{V}\cdot\mathbf{F} \qquad \ldots(4)$$

where $V^2/2$ = kinetic energy per unit mass

gz = potential energy per unit mass due to field of gravity.

The first term in the right hand side of the equation represents the work done on a unit mass of air per unit time by pressure force; and the second term, the work done per unit time on a unit mass of air by force of friction. The Coriolis force does no work, i.e. $(-2\mathbf{\Omega} \times \mathbf{V})\cdot\mathbf{V} = 0$.

To obtain the equation of energy per unit volume, we multiply the original equation of motion (3) by $\rho\mathbf{V}$ (ρ = density, $\mathbf{V}$ = velocity) to arrive, after some modification and transformation, at the form

$$\frac{d}{dt}\left(\rho\frac{V^2}{2}\right) - \frac{V^2}{2}\frac{d\rho}{dt} = -\nabla\cdot(P\mathbf{V}) + P\nabla\cdot\mathbf{V} + \rho\mathbf{V}\cdot\mathbf{F} + \rho\mathbf{V}\cdot\mathbf{g} \qquad \ldots(5)$$

Using the equation of continuity $-\frac{1}{\rho}\frac{d\rho}{dt} = \nabla\cdot\mathbf{V}$ and substituting it in the above equation, we get

$$\frac{\partial E}{\partial t} + \mathbf{V}\cdot\nabla E + E\nabla\cdot\mathbf{V} = -\nabla\cdot(P\mathbf{V}) + P\nabla\cdot\mathbf{V} + \rho\mathbf{V}\cdot\mathbf{F} + \rho\mathbf{V}\cdot\mathbf{g} \qquad \ldots(6)$$

where $E = \rho V^2/2$ is the kinetic energy per unit volume.

The velocity $\underline{V}$ has its three rectangular components $\underline{u}$, $\underline{v}$, and $\underline{w}$ directed along $\underline{x}$ (zonal), $\underline{y}$ (meridional), and $\underline{z}$ (upward) coordinates respectively. Since in most cases, as far as atmospheric motions are concerned, the vertical component is of very much smaller magnitude compared with the horizontal components, we will confine our measurements of total kinetic energy to zonal and meridional motions. The equation of kinetic energy per unit mass is thus expressed as:

$$\text{K.E.} = V^2/2 = \frac{1}{2}(u^2 + v^2).$$

Computations of Zonal and Meridional Components of Kinetic Energy

Average value of kinetic energy per unit mass around a latitude circle:

$$\text{K.E.} = \frac{1}{2\pi}\int_0^{2\pi}\left(\frac{u^2 + v^2}{2}\right) d\lambda = \frac{1}{2}\,\overline{(u^2 + v^2)}^{\lambda} \qquad \ldots(7)$$

Making geostrophic assumptions, we have

$$u = -\frac{g}{f}\frac{\partial z}{\partial y} = -\frac{g}{f}\frac{1}{a}\frac{\partial z}{\partial \phi}$$

$$u^2 = \left(\frac{g}{af}\right)^2 \left(\frac{\partial z}{\partial \phi}\right)^2 = C(1)\left(\frac{\partial z}{\partial \phi}\right)^2$$

$$v = \frac{g}{f}\frac{\partial z}{\partial x} = \frac{g}{f}\frac{1}{a\cos\phi}\frac{\partial z}{\partial \lambda}$$

$$v^2 = \left(\frac{g}{af}\right)^2 \frac{1}{\cos^2\phi}\left(\frac{\partial z}{\partial \lambda}\right)^2 = \frac{C(1)}{\cos^2\phi}\left(\frac{\partial z}{\partial \lambda}\right)^2$$

where . . . .

g = gravitational constant

f = Coriolis parameter

Z = geopotential height, 500 mb surface

a = mean radius of the earth

ϕ = latitude

λ = longitude

$C(1) = (g/af)^2$

Substituting these values of $\underline{u}^2$ and $\underline{v}^2$ in equation (7):

$$K.E. = \frac{C(1)}{2} \overline{\left[\left(\frac{\partial z}{\partial \phi}\right)^2 + \frac{1}{\cos^2\phi} \left(\frac{\partial z}{\partial \lambda}\right)^2 \right]}^{\lambda} \qquad \ldots (8)$$

The height $\underline{Z}$ of a constant pressure surface specified along a given latitude ϕ is single-valued and finite, can be considered as a regularly behaving function of the longitude $\underline{\lambda}$. The Fourier series expansion for $\underline{Z}$ is

$$\begin{aligned} Z(\lambda) &= A_o + A_1 \cos\lambda + A_2 \cos 2\lambda + \ldots + A_n \cos n\lambda \\ &\quad + B_1 \sin\lambda + B_2 \sin 2\lambda + \ldots + B_n \sin n\lambda \\ &= A_o + \sum_n (A_n \cos n\lambda + B_n \sin n\lambda) \\ &= A_o + \sum_n C_n \cos(n\lambda - \theta_n) \end{aligned}$$

where

$$C_n = (A_n^2 + B_n^2)^{\frac{1}{2}}$$

$$\theta_n = \arctan \frac{Bn}{An}$$

The coefficients A_o, A_n, and B_n for 36 equi-spaced grid points around a latitude circle are evaluated as:

$$A_o = \frac{1}{36} \sum_1^{36} Z_N$$

$$A_n = \frac{1}{18} \sum_1^{36} Z_N \cos n\lambda_N$$

$$B_n = \frac{1}{18} \sum_1^{36} Z_N \sin n\lambda_N$$

Taking the partial derivatives of Z, expressed as a Fourier series expansion, with respect to ϕ and λ separately, we have

$$Z = A_o + \sum_n A_n \cos n\lambda + \sum_n B_n \sin n\lambda$$

$$\frac{\partial z}{\partial \phi} = \frac{\partial A_o}{\partial \phi} + \sum_n \frac{\partial A_n}{\partial \phi} \cos n\lambda + \sum_n \frac{\partial B_n}{\partial \phi} \sin n\lambda$$

$$\left(\frac{\partial z}{\partial \phi}\right)^2 = \left(\frac{\partial A_o}{\partial \phi} + \sum_n \frac{\partial A_n}{\partial \phi} \cos n\lambda + \sum_n \frac{\partial B_n}{\partial \phi} \sin n\lambda\right)^2$$

$$= \left(\frac{\partial A_o}{\partial \phi}\right)^2 + \left(\sum_n \frac{\partial A_n}{\partial \phi} \cos n\lambda\right)^2 + \left(\sum_n \frac{\partial B_n}{\partial \phi} \sin n\lambda\right)^2$$

$$+ 2\,(\text{all cross products})$$

Using properties of orthogonal functions, all the cross products will vanish in the integration over λ, and the equation is further reduced to

$$\overline{\left(\frac{\partial z}{\partial \phi}\right)^2} = \left(\frac{\partial A_o}{\partial \phi}\right)^2 + \frac{1}{2}\sum_n \left[\left(\frac{\partial A_n}{\partial \phi}\right)^2 + \left(\frac{\partial B_n}{\partial \phi}\right)^2\right] \qquad \ldots(10)$$

With respect to λ, we have

$$\frac{\partial z}{\partial \lambda} = \sum_n n\,(B_n \cos n\lambda - A_n \sin n\lambda)$$

$$\left(\frac{\partial z}{\partial \lambda}\right)^2 = \left[\sum_n n\,(B_n \cos n\lambda - A_n \sin n\lambda)\right]^2$$

$$\overline{\left(\frac{\partial z}{\partial \lambda}\right)^2} = \frac{1}{2}\sum_n n^2 \left(B_n^2 + A_n^2\right) = \frac{1}{2}\sum_n n^2 C_n^2$$

Therefore:

$$(\text{K.E.})_u = \frac{1}{2}\, C(1)\, \overline{\left(\frac{\partial z}{\partial \phi}\right)^2}$$

$$= \frac{C(1)}{4}\left[2\left(\frac{\partial A_o}{\partial \phi}\right)^2 + \sum_n \left(\frac{\partial A_n}{\partial \phi}\right)^2 + \sum_n \left(\frac{\partial B_n}{\partial \phi}\right)^2\right] \qquad \ldots(11)$$

$$(K.E.)_v = \frac{C(1)}{2\cos^2\phi}\,\overline{\left(\frac{\partial z}{\partial \lambda}\right)^2}$$

$$= \frac{C(1)}{4\cos^2\phi}\sum_n n^2 C_n^2$$

where $\qquad C(1) = \left(\frac{g}{af}\right)^2$

Summing up the zonal and the meridional kinetic energy components, we get in finite difference form:

$$(K.E.)_{u+v} = \frac{C(1)}{4}\left[2\left(\frac{\Delta A_o}{\Delta\phi}\right)^2 + \sum_n\left(\frac{\Delta A_n}{\Delta\phi}\right)^2 + \sum_n\left(\frac{\Delta B_n}{\Delta\phi}\right)^2 + \sum_n \frac{n^2}{\cos^2\phi}\, C_n^2\right] \qquad \ldots(12)$$

<u>Computations of Kinetic Energy Ring and Zone Values</u>

The equation for the value of kinetic energy per unit mass around a latitude circle can be altered accordingly to give kinetic energy per mb for a zonal ring of width $\Delta\phi$, thus,

$$(K.E.)_{ring} = \frac{\pi g\cos\phi}{8\Omega^2(\Delta\phi)\sin^2\phi}\left[2(\Delta A_o)^2 + \sum_n\left[(\Delta A_n)^2 + (\Delta B_n)^2\right] + \frac{(\Delta\phi)^2}{\cos^2\phi}\sum_n n^2 C_n^2\right] \qquad \ldots(13)$$

where the first term in the bracketed expression is the zonal mean flow energy followed by the <u>u</u> and <u>v</u> components of the perturbation energy.

The limited hemisphere (20 - 90 degrees) was divided into seven rings and four zones as shown:

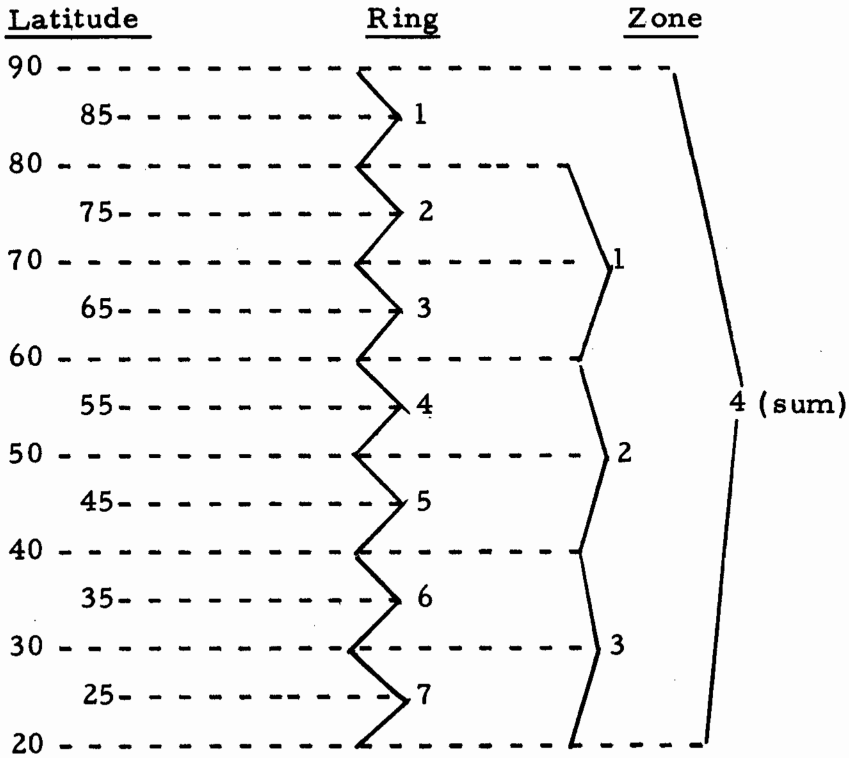

The weightings used for the evaluation of each ring are as follows:

$$\text{for} \qquad (KE)_v \text{ Ring } 7 = \frac{1}{4}(ke_1 + 2ke_2 + ke_3)$$

$$(KE)_u \text{ Ring } 7 = ke_{1\frac{1}{2}} + ke_{2\frac{1}{2}}$$

where the numerical subscripts represent the indicated levels shown hereunder:

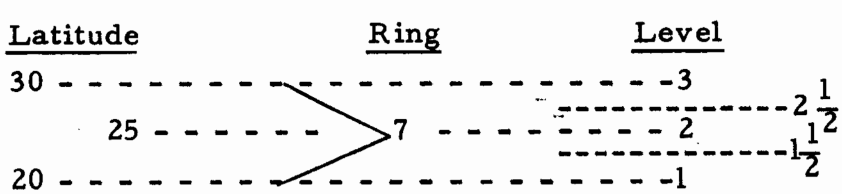

The weightings used for the evaluation of each zone (for both components of K.E.) are much simpler; we have

(KE) Zone 1 = KE (Ring 2 + Ring 3)
(KE) Zone 4 = KE (Ring 1 + Ring 2 + ... + Ring 7).
= KE (Ring 1 + Zones 1, 2, and 3).

To compensate for the successive reductions of the volume of the latitudinal rings as one goes poleward, a normalisation factor, the cosine of the latitude, is often introduced. In this study the factor automatically appears in the ring values of the kinetic energy (13).

Computations of Kinetic Energy of the Mean

Kinetic energy of the mean is distinguished from mean kinetic energy in that while the latter is the average kinetic energy for the month ($1/30 \sum_{1}^{30} (KE)_d$), the former is the kinetic energy based on mean "Z" values ($1/30 \sum_{1}^{30} Z_d$) for each grid point.

Likewise, the ring and zone values of the mean were obtained and similarly distinguished from mean ring and zone values.

In the evaluation of the monthly mean values of kinetic energy for u and v components, the mean zonal flow energy was isolated and compared with the mean perturbation energy spread in wave numbers one to fifteen for both u and v.

The latitudinally-averaged geopotential heights of the mean map were computed to obtain the deviations for each point in the grid to have a quantitative measure of the energy of the stationary or standing waves and the moving or transient waves.

EVALUATIONS OF THE RESULTS

The computer programming was written to specify an output which included the following:

(i) Daily output of Fourier coefficients (amplitude), $(nC)^2$.. .. a proportionate measure of the v component of the kinetic energy, and the phase angle θ, for each wave number from 0 to 15 and for each fifth-degree latitude from 20 degrees to the pole.

(ii) Daily output of ring and zone values of u and v components of the kinetic energy for all wave numbers.

(iii) Monthly mean height field.

(iv) Monthly mean ring and zone values of u and v components of the kinetic energy for all wave numbers.

(v) Fourier coefficients, $(nC)^2$, and the phase angles with the monthly mean height field as the input data.

(vi) Likewise, the corresponding ring and zone values of u and v components of the kinetic energy of the mean.

All these aforementioned outputs of the computer were obtained separately for both the northern and southern hemispheres.

Amplitude Spectra

A day-to-day amplitude evaluation from September 1 to 30 for both hemispheres shows that significant contributions of each harmonic wave are confined only to wave numbers 1 to 10 for all latitudinal rings. Much higher harmonics are considered to lie within the noise level.

Figures 4 and 5 show the amplitude spectra of the mean in northern hemisphere. At latitudes 20 to 45, the peak value is at wave number one decreasing generally up to wave number 10. Two distinct amplitude maxima are found at wave numbers 2 and 4 from latitudes

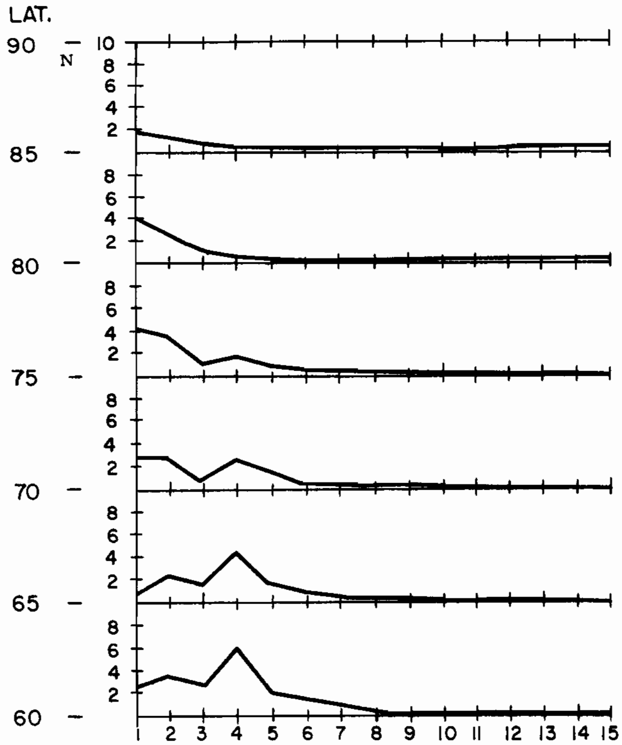

Fig. 4

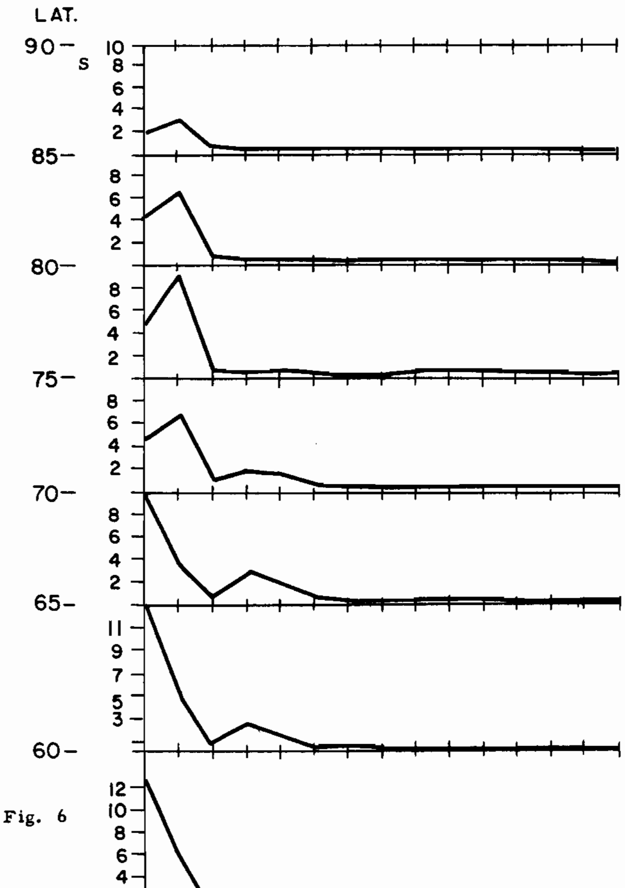

Fig. 6

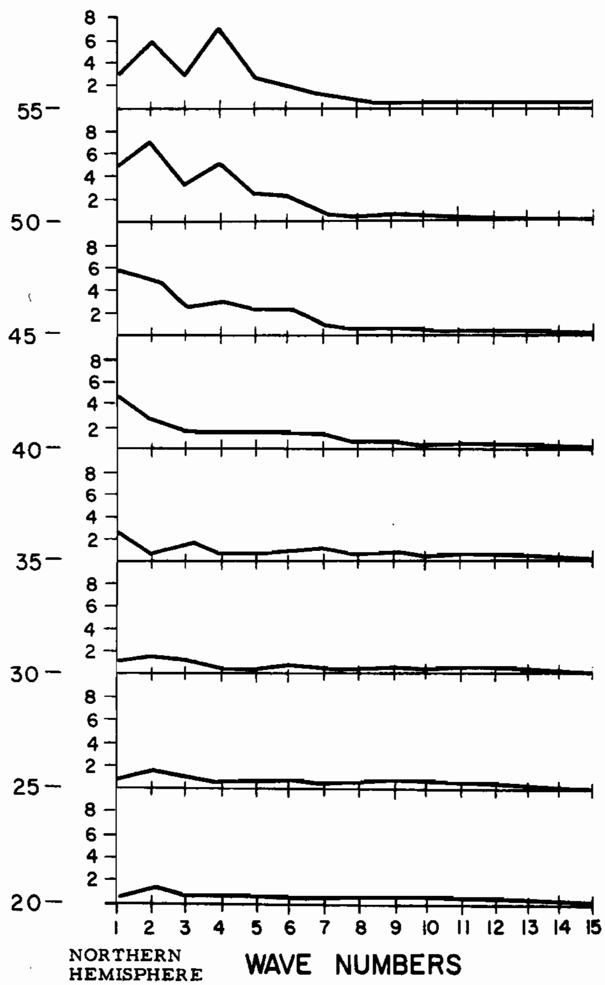

Fig. 5

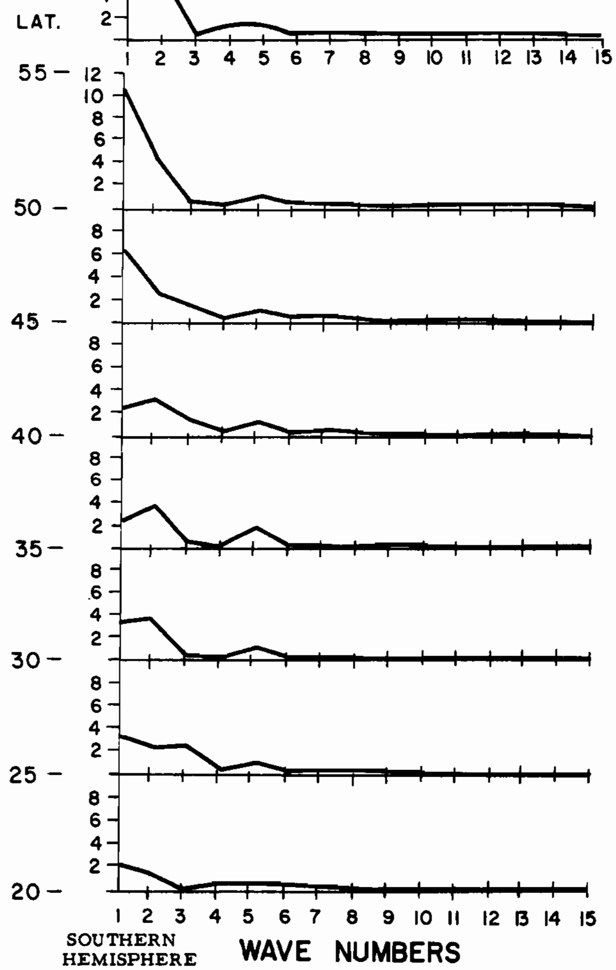

Fig. 7

FIGS. 4,5,6,7,— AMPLITUDE SPECTRA OF THE 500 MB. MEAN FOR SEPTEMBER, 1957. UNITS — 10 METERS.

50 to 75. Higher latitudes show gradual decrease in amplitude from wave number one.

In the southern hemisphere, as shown in Figures 6 and 7, the amplitude peak fluctuates between wave numbers 1 and 2. It is at number 2 at latitudes 35, 40, and 70 to 85, and at number 1 in all the other measured latitudes. Moreover, secondary maxima are exhibited prominently at wave number 5 at latitudes 20 to 55. Minimum discrete values are found at wave number 4 at latitudes 20 to 50 and at wave number 3 at latitudes 55 to 85.

Almost in all latitude belts the amplitude values in the southern hemisphere are relatively greater than those of the northern hemisphere.

Time Cross-sections of Zonal Flow Energy

Daily amounts of zonal flow energy were plotted and graphed for each 20-degree latitudinal zone for both hemispheres. Figures 8 and 9 show the energy time cross-sections for northern and southern hemispheres respectively.

By a glance at the graphs, one can readily see that the mean zonal energy at the southern hemisphere is very much greater than that of the northern hemisphere at all latitudinal belts. The uppermost part of each Figure shows the total energy for the entire hemispheric zone (20 degrees to 90 degrees). The relative comparison shows that the zonal energy of the northern hemisphere is roughly one third of that of the southern hemisphere.

Since the month of September falls on different seasons for each hemisphere, an effort was made to compare the September value of the southern hemisphere with the March value of the northern hemisphere (from Boville, 1961). This comparison showed the zonal flow energies for March and September in the northern hemisphere are approximately of the same magnitude and the inter-hemispheric ratio

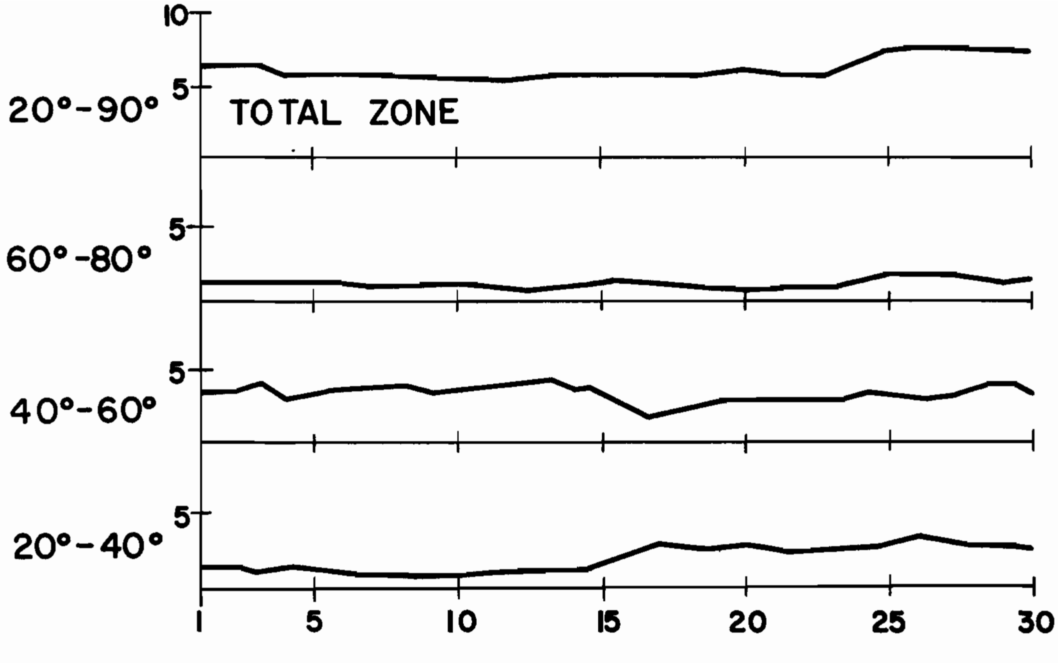

FIGURE 8. TIME CROSS-SECTIONS OF ZONAL FLOW ENERGY FOR EACH 20 DEGREE ZONE IN THE NORTHERN HEMISPHERE UNITS, 10^{16} JOULES MB^{-1}.

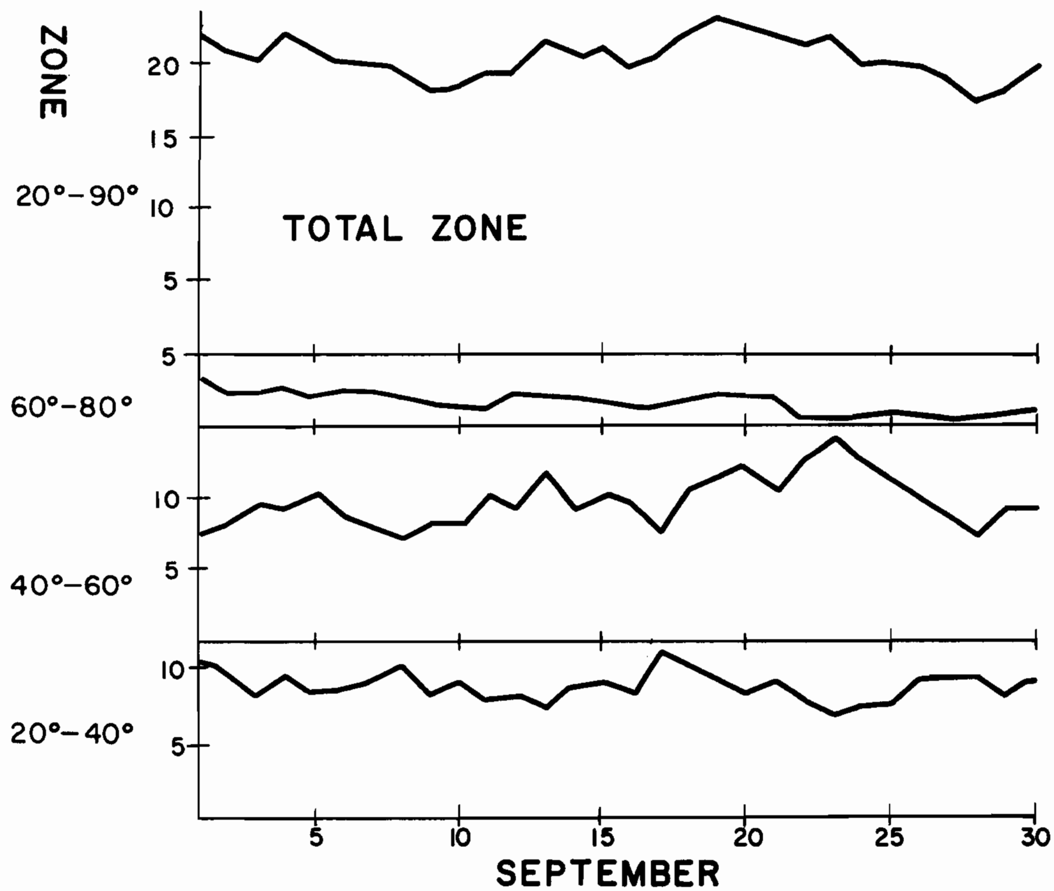

FIGURE 9. TIME CROSS-SECTIONS OF ZONAL FLOW ENERGY FOR EACH 20 DEGREE ZONE IN THE SOUTHERN HEMISPHERE. UNITS, 10^{16} JOULES, MB^{-1}.

of one third thus remained essentially the same.

The fact that the northern hemisphere has a higher percentage of land areas than the southern hemisphere would not seem to explain this disparity in zonal energy amounts because 500 mb level is well above the friction layer. However, this difference in land masses taken in a different light would probably support the contention that land areas are thermal sources of upward heating and could bring about meridional heat transport creating less temperature gradient. Ultimately, this sets up wider height contours and less mean wind.

It is quite remarkable that in both hemispheres, zone 60 to 80 shows the least amount of zonal energy while zone 40 to 60 exhibits greatest amounts. This is to be expected, though, because of their zone area differences. However, while the energy at the lowest latitude zone (20 - 40) has remained high in the southern hemisphere, it has gone down in the northern hemisphere.

Time Cross-sections of Perturbation Energy

In the total kinetic equation that was derived in a previous section

$$(K.E.)_{u+v} = \frac{C(1)}{4(\Delta \phi)^2} \left[2(\Delta A_o)^2 + \sum_n \left[(\Delta A_n)^2 + (\Delta B_n)^2 \right] + \sum_n \frac{n^2 (\Delta \phi)^2}{\cos^2 \phi} (A_n^2 + B_n^2) \right] \qquad \ldots (14)$$

the first summation term in the bracketed expression gives us a measure of the u component of the eddy energy, and the last summation term, of the v component of the eddy energy.

The daily algebraic sums of these two components taken from the printed output were plotted and delineated on a time cross-section chart. The contributions of the dominant waves (one to three) were graphed and are shown in Figures 10 and 11 for northern and southern hemispheres respectively.

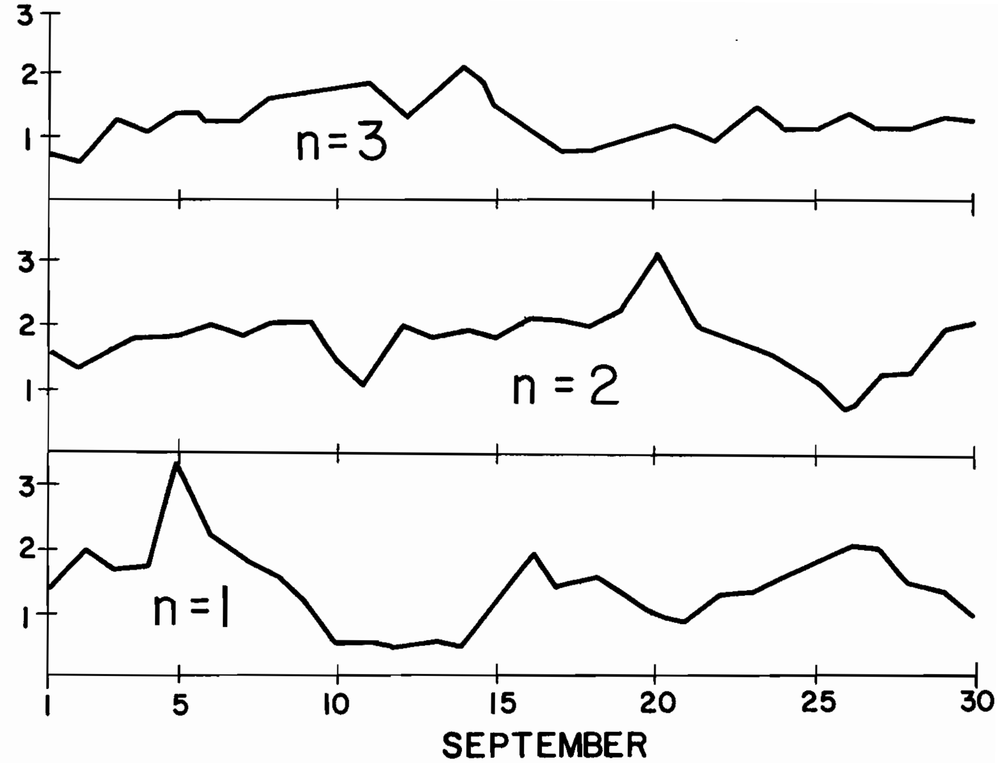

FIGURE 10. TIME CROSS-SECTIONS OF PERTURBATION ENERGY FOR THE FIRST THREE WAVE NUMBERS IN THE NORTHERN HEMISPHERE.

UNITS, 10^{16} JOULES MB^{-1}.

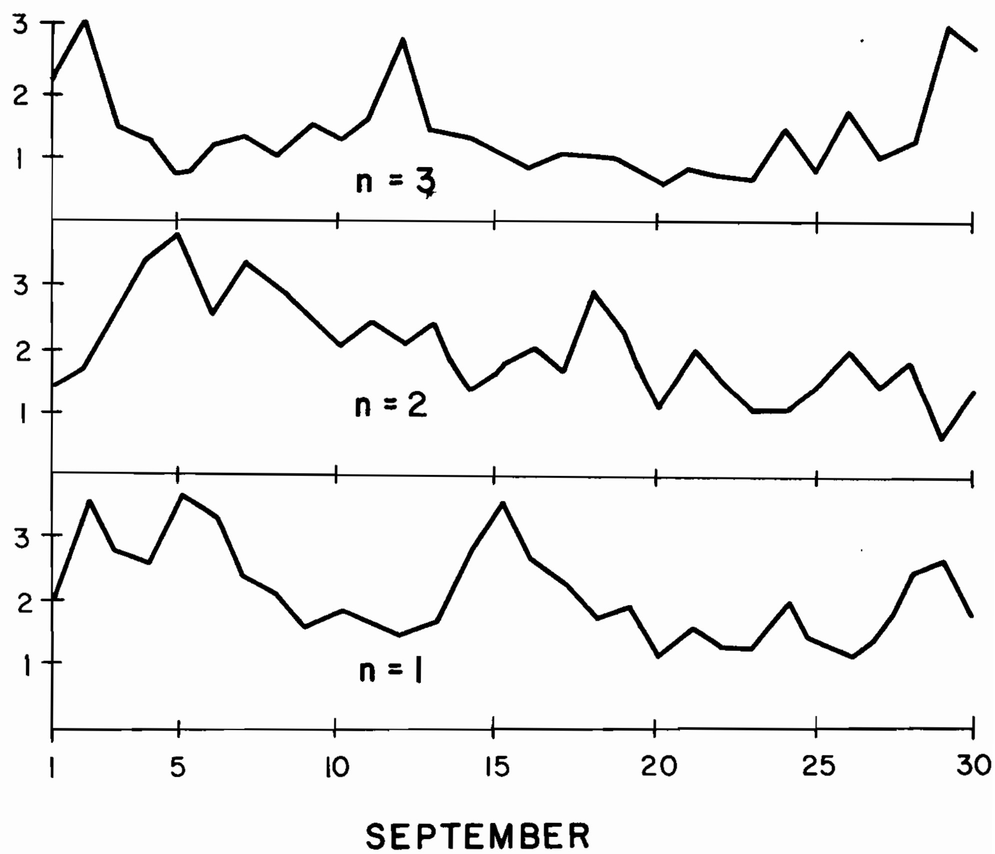

FIGURE 11. TIME CROSS-SECTIONS OF PERTURBATION ENERGY FOR THE FIRST THREE WAVE NUMBERS IN THE SOUTHERN HEMISPHERE.

UNITS, 10^{16} JOULES MB^{-1}.

In the northern hemisphere, energies at wave numbers 2 and 3 show less fluctuations, while the values at wave number one show a wider range.

In the southern hemisphere, the energy curves in all wave numbers do not show any definite trend, implying the time variation of the contributions is not a steady factor.

In the over-all picture of the two hemispheres, it can be deduced that the total contributions of all the first three dominant harmonics are practically of the same magnitude. It will be seen later in this paper that if the total kinetic energy (zonal flow and perturbation) of the two hemispheres varies by quite a significant amount - in the magnitude of 1 to 3 - the difference is mostly confined to the zonal flow and quite an unappreciable quantity in the perturbation component.

Eddy Energy Components as a Function of Zonal Wave Numbers

The monthly mean of the perturbation energy for both horizontal components for all wave numbers for all latitudinal zones are transcribed from the tabulated output values (Tables I and II) to spectral graphs shown in Figures 12 and 13.

In the graph for northern hemisphere, the eddy energy amounts in all zones show peak values at wave numbers 2 and 4, and are gradually decreasing in the direction of the short waves. By zones, the belt of 40N - 60N appears to be the path of strong perturbations. This is expected in view of the fact that this is the alley of the transient cyclones which we often see in the synoptic maps at this time of the year.

The u component appears to be more dominant in the first three long waves while the v component seems to be greater from wave number 5 to the end of the short wave spectrum. It indicates that the perturbation waves are more flattened in the long wave part of the

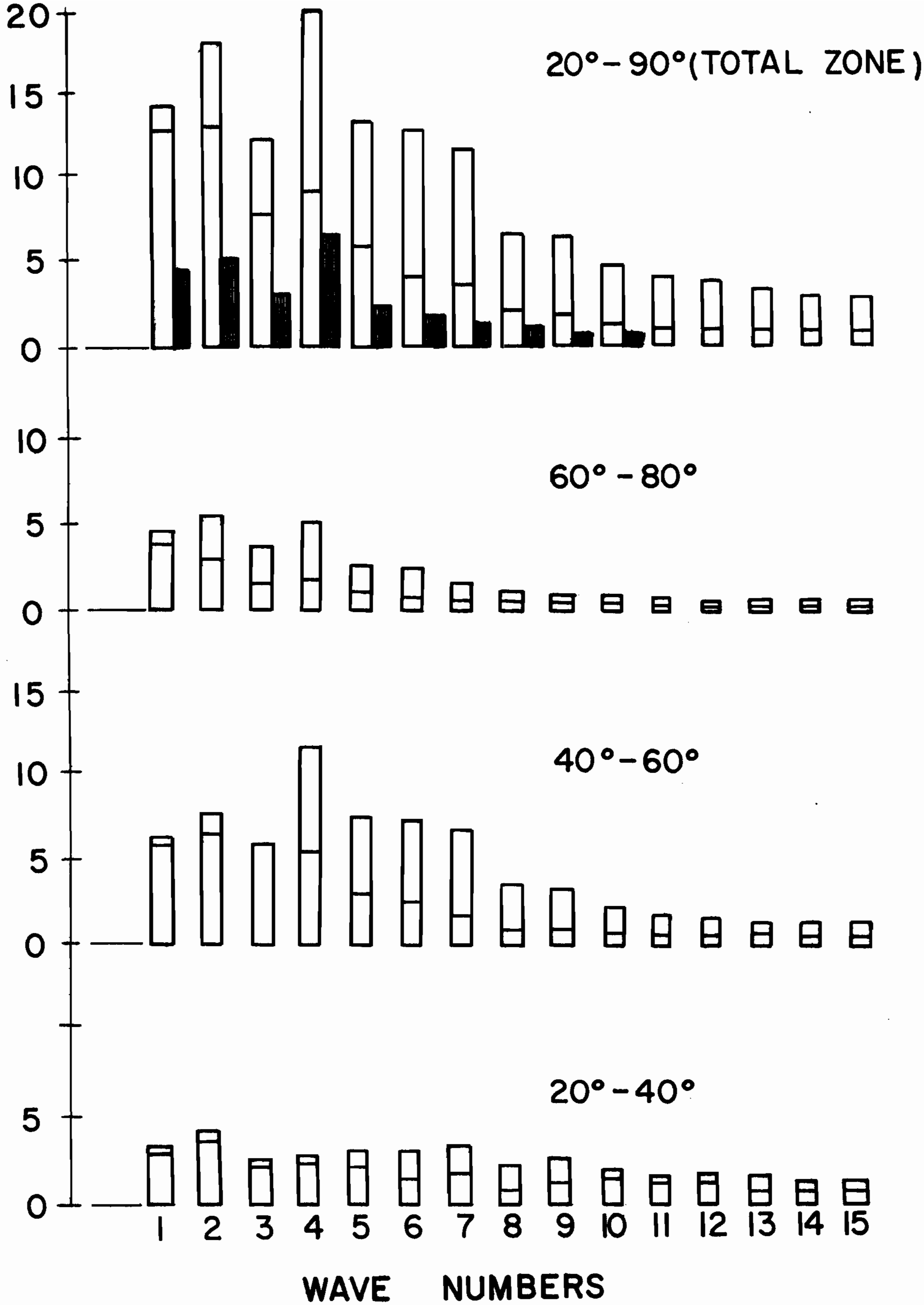

Figure 12. Spectral distribution of perturbation energy in the northern hemisphere. The lower part of the columns represent the u component; and the upper part, the v component. In the total zone, the standing waves have been added as shaded columns.

Units, 10^{15} joules mb^{-1}.

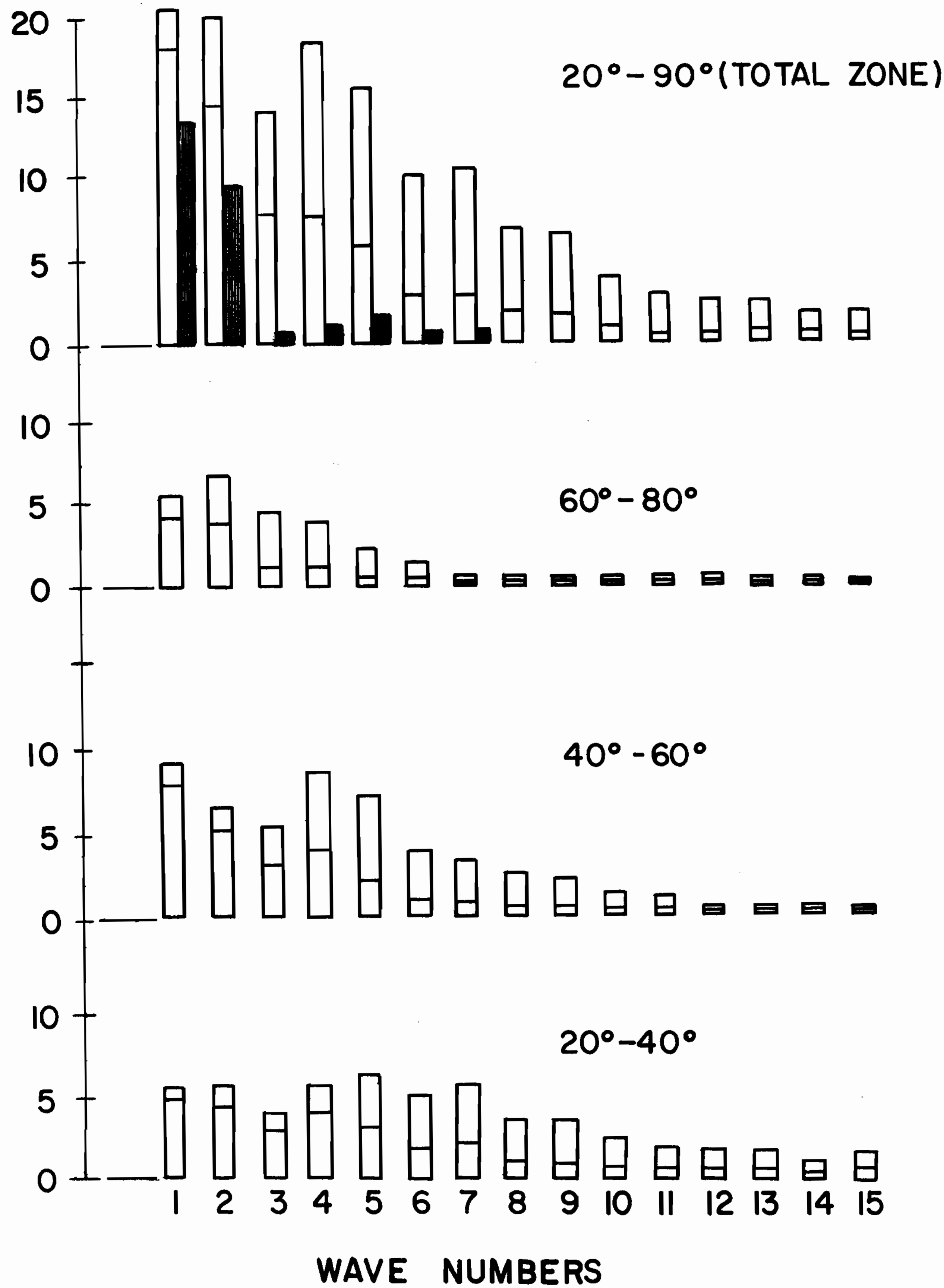

Figure 13. Spectral distribution of perturbation energy in the southern hemisphere. The lower part of the column represents the u component; and the upper part, the v component. In the total zone, the standing waves have been added as shaded columns.

Units, 10^{15} joules mb^{-1}.

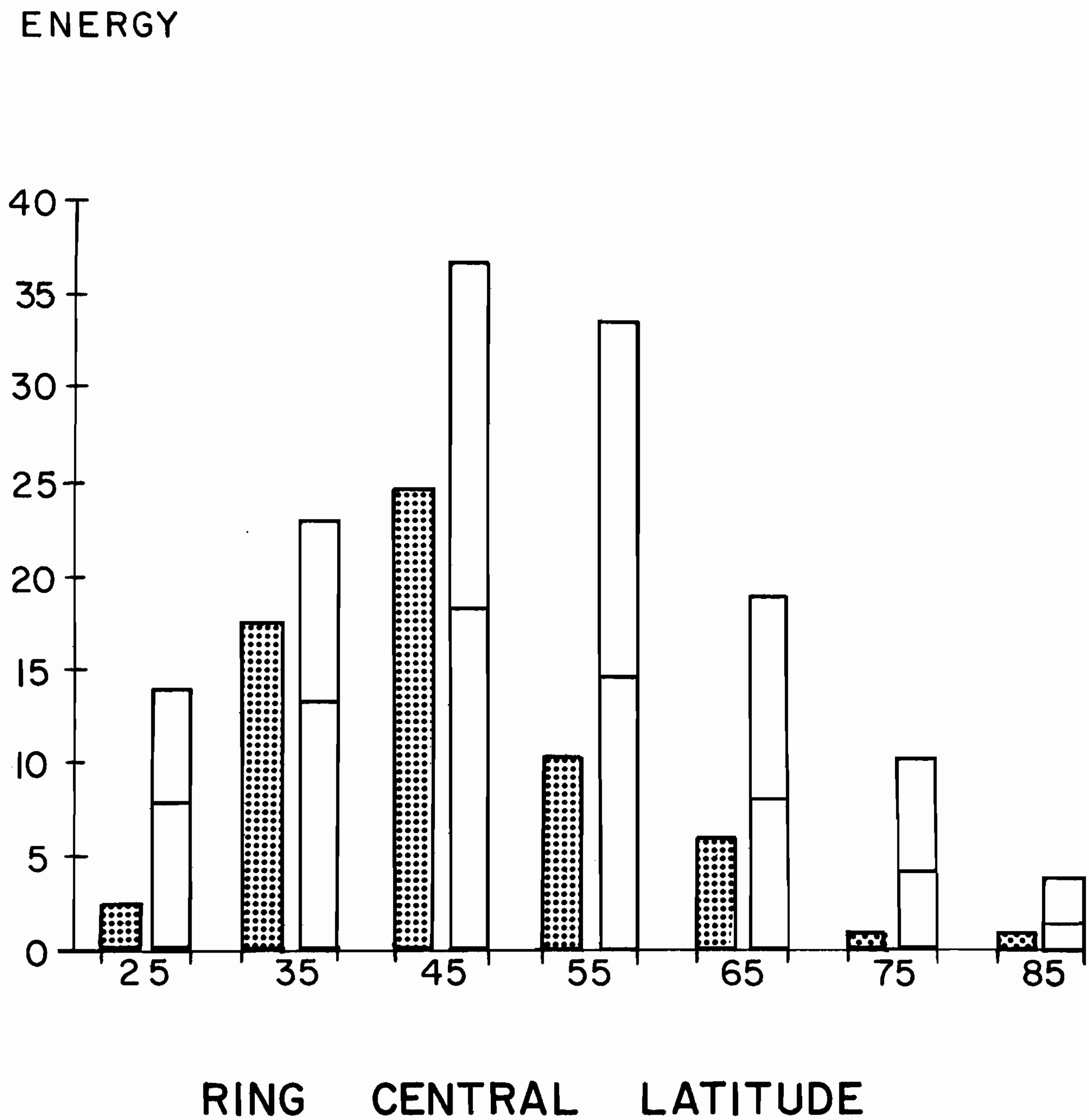

Figure 14. Latitudinal ring profiles of monthly mean zonal and perturbation energy for the northern hemisphere. The shaded columns represent the zonal flow energy; the plain columns, the perturbation energy (lower part, u component; upper part, v component).

Units, 10^{15} joules mb^{-1}.

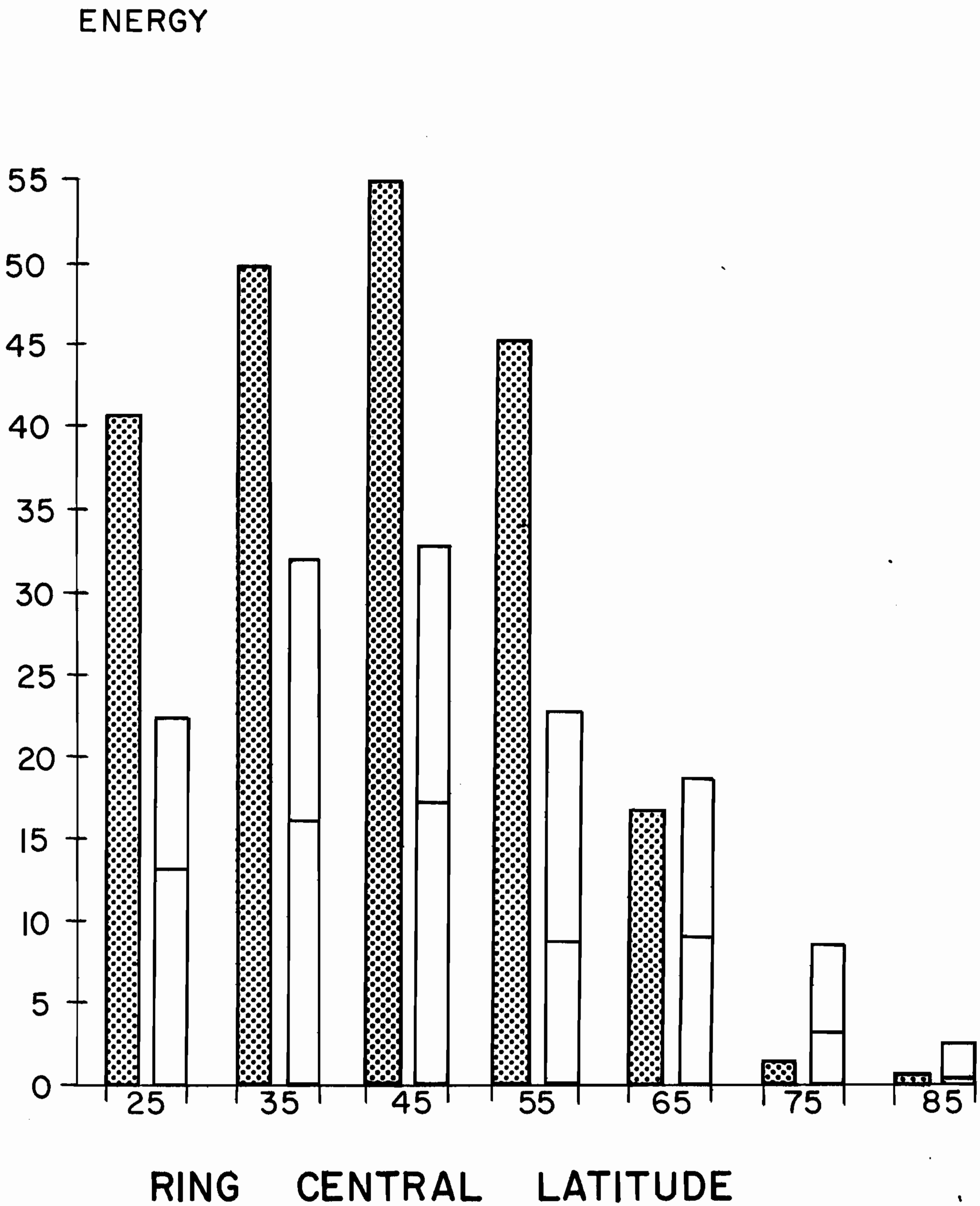

Figure 15. Latitudinal ring profiles of monthly mean zonal and perturbation energy for the southern hemisphere. The shaded columns represent the zonal flow energy; the plain columns, the perturbation energy (lower part, u component; upper part, v component).

Units, 10^{15} joules mb^{-1}.

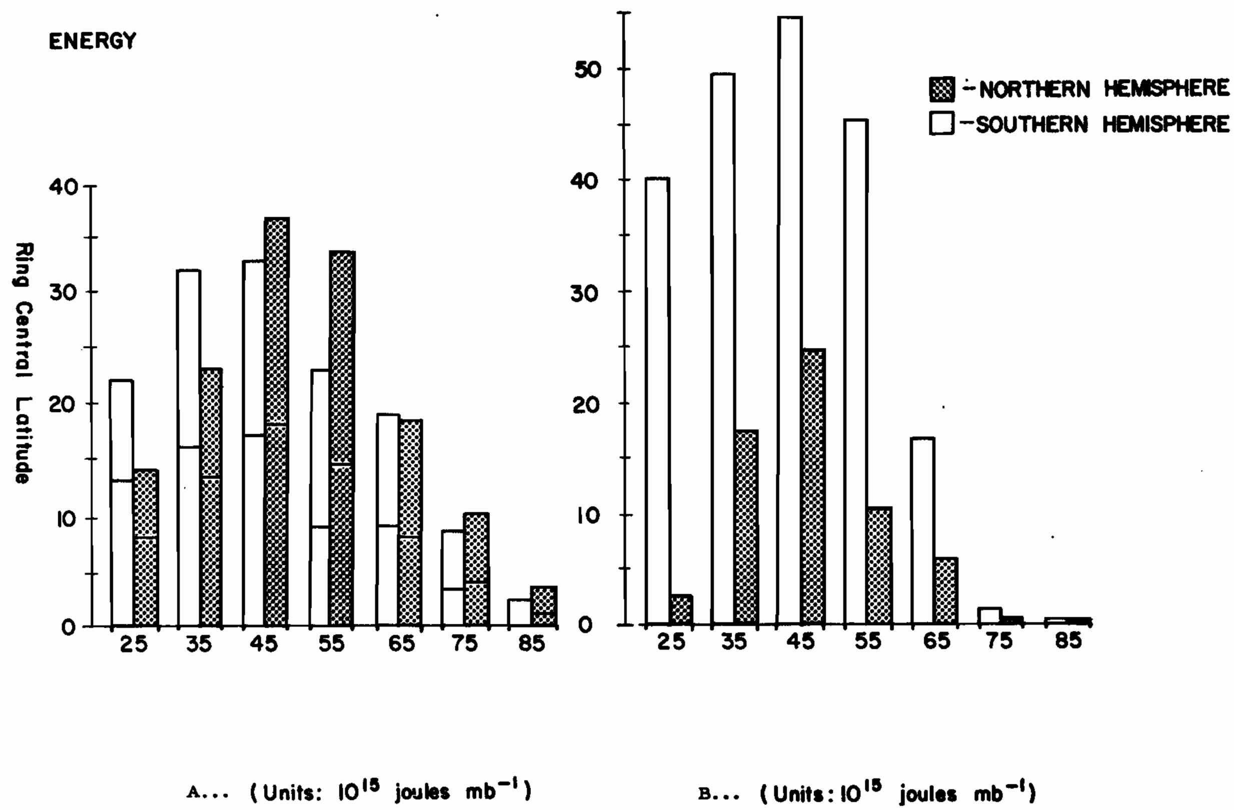

Figure 16. A - Ring profiles of mean perturbation energy for both hemispheres.
B - Ring profiles of monthly mean zonal energy for both hemispheres.

spectra and tend to bulge more at the medium and short wave ranges.

In the southern hemisphere the maximum values of the perturbation energy are mostly centered at wave numbers 1, 2, 4, and 5. As usual, the amounts slowly ebb down towards the higher wave numbers. There is some indication that the zone 40S - 60S is favoured for perturbations , but this is not marked as in the case of northern hemisphere . This may be due to the overwhelming predominance of water surface in the southern hemisphere which tends to smooth out atmospheric disturbances. As in the northern hemisphere, the u components predominate in the long waves and the v components in the medium and short waves.

In Figures 12 and 13 the shaded bars alongside the columns of total zone (20-90 degrees) values represent the energy of the standing waves for each particular wave number. These values, obtainable from the computer output, are the kinetic energy of the mean. The proportion of the eastward component to the northward component in these spectra is the same as that of the mean kinetic energy spectra; i. e. , the u component is relatively greater than the v component in quasi-stationary planetary waves and vice versa in the rest of the waves.

Table III shows the quantitative measurements of the energy of the standing waves in both hemispheres.

Latitudinal Ring Profiles for Monthly Mean Zonal and Perturbation Energy

A better scheme to show the comparative total amounts of mean zonal energy as contrasted with mean perturbation energy for all wave numbers is to graph their profiles as a function of latitude.

As shown in Figure 14, the zonal flow energy in the northern hemisphere is very much less than the eddy energy in all latitudinal rings, especially in the subtropic and polar regions. The ring, 40-50 degrees, shows pronounced activity from both zonal and meridional

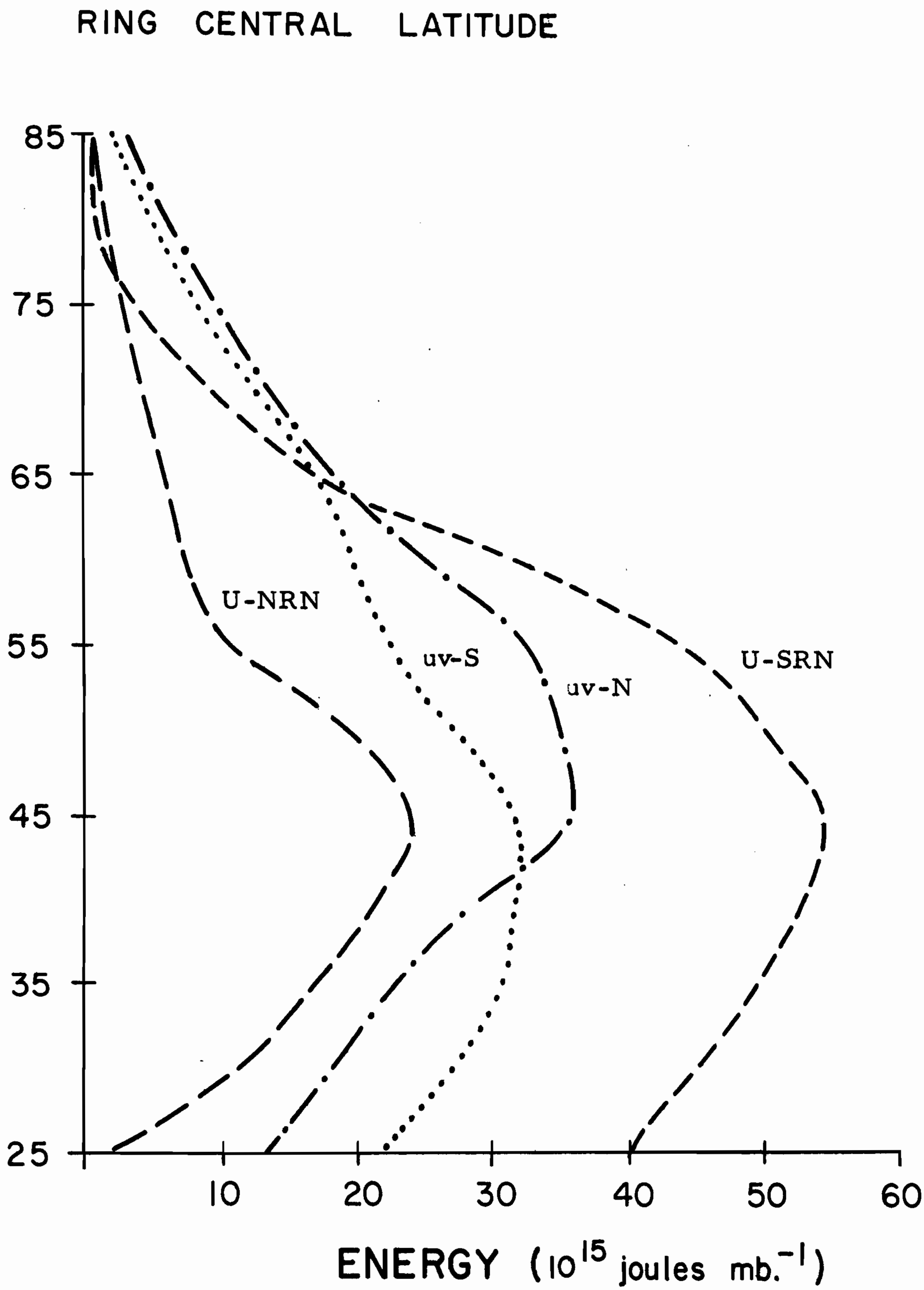

Figure 17. Composite picture of energy profiles in both hemispheres at 500 mb.

considerations. The zonal component of the perturbation energy appears to be greater than the meridional component equatorward and vice versa poleward of that ring.

By contrast, the spectrum in the southern hemisphere is diametrically opposite of that in the northern hemisphere. The zonal flow energy is very much greater than the eddy energy in all rings except in the subpolar areas. The u and v components of the perturbation for each ring are almost of the same quantity, and show decreasing tendency towards the pole. Like in the northern hemisphere, the maximum peaks are found in the middle latitudes where westerlies and cyclonic disturbances are proportionately more and more intense. Figure 15 shows the spectrum in the southern hemisphere.

In Figure 16, the comparison of the kinetic energy profiles of the two hemispheres is shown side by side with the zonal mean flow and the perturbation energy in separate diagrams. Table IV gives the individual ring energy values and their total.

It is very remarkable that the big difference of total kinetic energy between the two hemispheres is mostly concentrated in the zonal flow branch and significantly negligible in the eddy portion.

Figure 17 provides a composite picture of the energy profiles in both hemispheres showing clearly the relative differences for each component.

Energy of Standing and Transient Waves

After plotting the monthly mean values of perturbation energy with the latitudinal rings as the ordinate and the wave numbers as the abscissa, isopleths of energy were drawn with spacings of 10^{15} joules mb^{-1}.

Figures 18 and 19 show the total perturbation energy isopleths for the northern and southern hemispheres. The center of maximum energy, spread meridionally, (exact value at center - 6.2

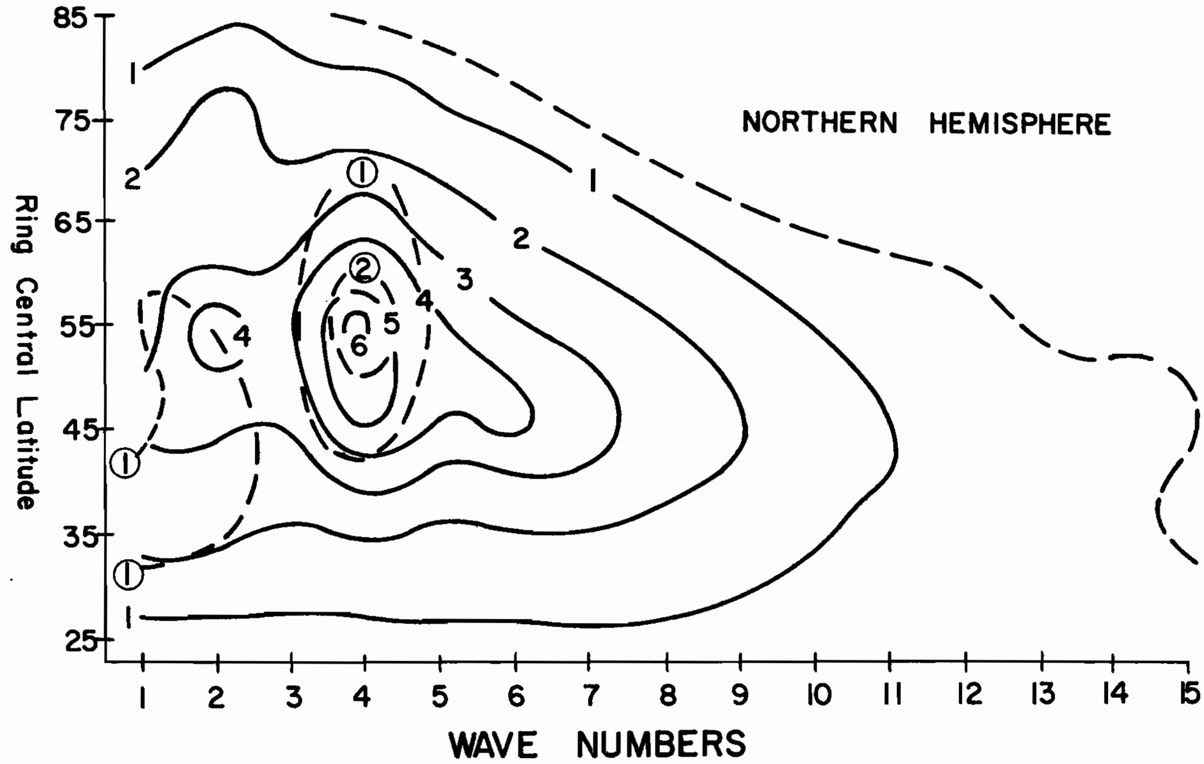

FIGURE 18. ENERGY ISOPLETHS OF STANDING WAVES (DASHED LINES) AND TOTAL PERTURBATION ENERGY (FULL LINES).
UNITS, 10^{15} JOULES MB^{-1}.

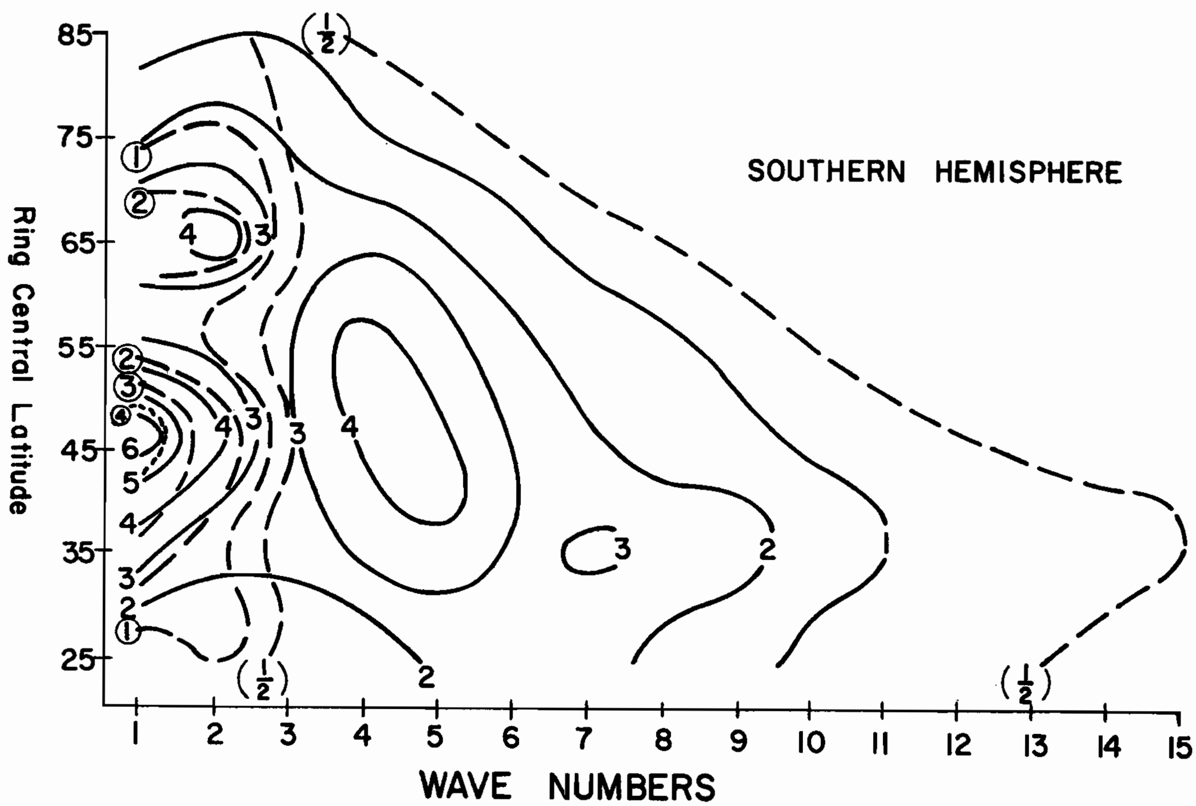

FIGURE 19. ENERGY ISOPLETHS OF STANDING WAVES (DASHED LINES) AND TOTAL PERTURBATION ENERGY (FULL LINES).
UNITS, 10^{15} JOULES MB^{-1}.

times 10^{15} joules mb^{-1}) seems to be concentrated at the 40N - 60N zone at wave number 4 in the northern hemisphere. Secondary peaks (values of 4.0×10^{15} joules mb^{-1}) are also found at wave numbers two and six in the same latitudinal belt. The general trend of the succeeding isolines is to be stretched along the direction of increasing harmonics with axis at the 40 - 50 degree ring. Very small amounts of energy are found beyond wave number 10 in lower latitudes, beyond wave number 11 in middle latitudes, and beyond wave number 8 in polar latitudes.

For the southern hemisphere (Figure 19) the energy concentration lies at ring 40S - 50S with pronounced maximum at wave number one. There are secondary maxima at 60S-70S ring at wave numbers 2 and 4 at the latitude belt of 40S-60S. The distribution of energy along the harmonics spread and latitudinal direction is remarkably similar with that of the northern hemisphere.

The next step in our analysis is to plot along the same scale of grid the kinetic energy of the monthly mean to represent the standing waves, i.e., not changing with respect to time or stationary. The curves are shown as dashed lines in the preceding graphs. In the northern hemisphere, the center of energy concentration of the standing waves (in the magnitude of 2.5×10^{15} joules mb^{-1}) is similarly located as the total energy center in the same isoplethal chart with distribution up to wave number five only and up to 70 degree latitude.

The energy of the standing waves in the southern hemisphere shows more or less a restricted pattern with major concentration at 40S - 50S ring and secondary peak at 60S - 70S belt mostly of wave number 1 extending to number two. It is quite obvious that wave numbers 3 to 15 do not contribute anything significant to the standing waves in this hemisphere.

Subtracting the kinetic energy of the standing waves from the total kinetic energy of the perturbations, we obtain the energy of the moving or transient waves. The results are shown in Figures 20

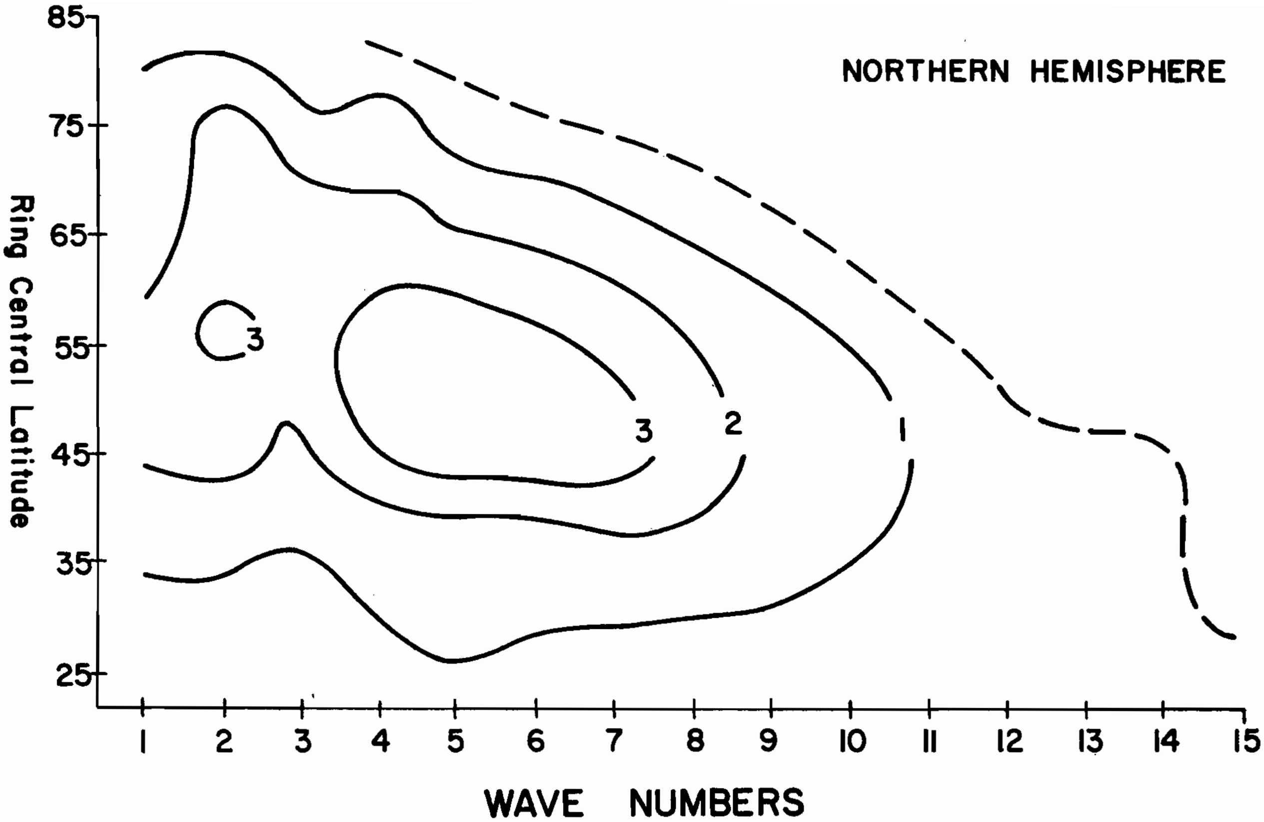

FIGURE 20. ENERGY ISOPLETHS OF TRANSIENT WAVES. UNITS, 10^{15} JOULES MB^{-1}.

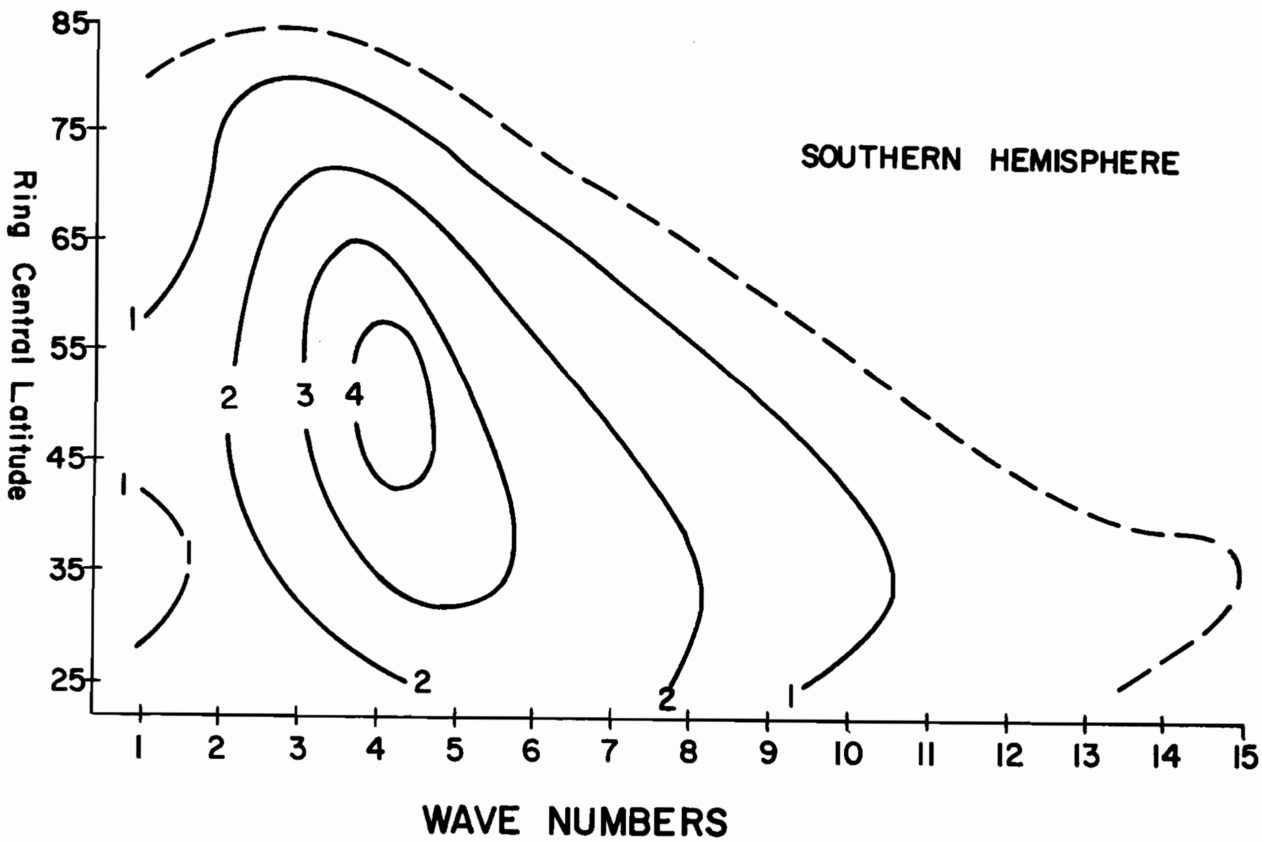

FIGURE 21. ENERGY ISOPLETHS OF TRANSIENT WAVES. UNITS, 10^{15} JOULES MB^{-1}.

and 21.

The isolines of the differential amounts in the northern hemisphere now show a broadening of the center pattern along the breadth of wave numbers, while the orientation of the whole structure remains essentially of the same configuration. In other words, the shape of the distribution of the total kinetic energy was not much disturbed, except at the wave region of intense energetics where the standing waves show profound effects. This goes to show that the main strength of the standing waves is localized at the same wave band where the intensity of the total energy is likewise centered.

In the southern hemisphere the heavy concentration of isopleths of the standing wave energy in the same latitudinal sector and wave number regime as of the total kinetic energy practically cancels them out in the latter to produce a pattern of transient waves devoid of strong energy centers, except the one that was located at wave number 4 which was not perturbed at all by the standing waves.

All these findings about the quantitative and qualitative aspects of the standing and transient waves seem to corroborate previous statements in this paper regarding high energy values at the 40 - 60 degree belt in both hemispheres because this is the corridor of strong westerlies and frequent cyclonic disturbances in both hemispheres with very slight deviations.

Monthly Mean Height Field

One of the items programmed in the IBM computer was the computation of the monthly mean values of Z (geopotential height) for each of the 540 grid points of each hemisphere. The actual printed output forms (Figures 22 and 23) were utilized for delineating the mean contours in an effort to represent them in an approximate mercator form with the meridians and parallels properly arrayed.

MEAN MONTHLY HEIGHT FIELD 1957 273 500 N.H. FIG. 22

LAT \ LONG	0	10	20	30	40	50	60	70	80	90	100	110	120	130	140	150	160	170
90	532.0	532.0	532.0	532.0	532.0	532.0	532.0	532.0	532.0	532.0	532.0	532.0	532.0	532.0	532.0	532.0	532.0	532.0
85	536.1	536.5	536.6	536.4	535.8	534.9	534.2	533.5	532.7	531.4	530.8	529.5	529.7	530.6	531.4	532.1	532.6	532.9
80	540.3	541.1	541.2	540.8	539.6	537.9	536.5	535.1	533.4	530.8	528.1	527.1	527.4	529.2	530.9	532.2	533.2	533.4
75	544.7	544.9	545.1	544.8	544.4	542.9	541.5	539.4	537.6	535.1	531.6	529.2	529.7	532.4	535.2	537.1	538.2	538.5
70	546.4	546.3	547.4	547.4	547.6	547.7	547.6	546.1	544.1	541.6	538.1	535.4	534.9	536.8	539.9	543.0	544.6	544.2
65	546.8	545.9	545.4	547.8	551.2	553.5	555.6	555.3	552.9	549.0	545.3	541.6	539.8	541.3	546.9	550.9	552.7	551.0
60	547.7	547.6	547.5	549.9	555.9	561.8	565.0	567.3	564.6	558.7	553.2	548.3	546.2	547.2	553.5	558.5	560.1	556.4
55	555.9	554.8	554.3	555.9	561.7	569.0	574.0	574.5	571.3	566.4	559.8	553.8	550.1	550.6	555.5	559.6	561.1	556.1
50	567.2	565.4	565.4	566.0	570.8	575.9	577.8	576.7	573.1	570.2	565.6	559.6	554.8	554.3	556.7	558.9	560.4	559.7
45	577.9	574.4	572.6	572.9	576.9	579.7	579.1	576.7	576.5	574.6	571.5	566.9	561.3	560.4	562.2	564.2	566.3	563.1
40	584.2	581.1	577.5	577.5	581.9	583.4	582.2	580.6	581.3	580.2	577.8	574.3	569.4	568.0	571.5	574.6	576.2	573.4
35	588.9	585.1	581.9	582.8	585.9	586.0	585.2	584.0	583.7	582.9	581.8	580.2	578.1	576.9	581.7	584.2	585.3	584.2
30	591.7	588.8	585.9	587.4	589.8	588.6	586.3	585.7	585.4	584.6	584.1	584.2	584.6	583.9	587.8	590.1	591.0	590.2
25	592.2	591.6	588.7	589.7	591.3	589.1	587.2	586.4	586.5	586.1	586.1	586.6	586.3	586.4	589.1	591.7	592.2	591.1
20	591.5	591.5	589.4	589.9	591.0	589.3	587.7	587.4	586.3	586.4	586.6	586.2	584.7	586.1	588.6	590.5	590.9	589.7

MEAN MONTHLY HEIGHT FIELD 1957 273 500 N.H.

LAT \ LONG	180	170	160	150	140	130	120	110	100	90	80	70	60	50	40	30	20	10
90	532.0	532.0	532.0	532.0	532.0	532.0	532.0	532.0	532.0	532.0	532.0	532.0	532.0	532.0	532.0	532.0	532.0	532.0
85	532.8	532.8	533.0	533.3	533.6	534.0	534.2	534.2	533.8	533.7	533.8	534.0	534.5	535.0	535.2	535.1	535.3	536.7
80	533.6	533.6	534.0	534.6	535.2	536.1	536.5	536.9	535.6	535.4	535.6	536.1	537.1	538.0	538.4	538.3	538.7	539.5
75	536.7	535.5	535.1	535.6	536.9	538.3	537.9	536.7	535.3	534.3	534.2	535.8	537.7	540.1	541.7	542.9	543.5	543.[illegible]
70	541.6	539.2	539.4	541.0	544.0	545.6	544.7	542.3	540.4	538.8	538.8	540.3	541.6	543.8	546.1	547.1	547.2	546.[illegible]
65	547.4	544.3	544.2	547.4	552.6	555.2	552.4	548.5	547.0	544.4	542.3	542.2	544.8	546.9	550.0	550.5	549.9	548.7
60	550.8	546.4	547.2	553.0	561.0	563.5	560.2	553.5	549.5	547.6	547.5	546.7	547.1	550.4	554.3	556.2	554.7	551.7
55	549.9	546.2	549.5	559.1	569.5	572.9	569.2	562.1	556.0	553.6	552.6	550.5	552.4	555.8	560.3	562.1	561.7	559.[illegible]
50	550.3	547.8	554.7	566.3	576.6	577.6	574.7	569.9	563.4	560.7	559.8	559.8	560.5	561.2	566.6	568.1	570.0	570.[illegible]
45	557.0	557.9	564.3	574.6	579.8	579.7	578.9	575.9	572.1	569.8	569.7	572.6	573.8	571.7	573.9	574.7	577.1	578.[illegible]
40	571.1	571.1	575.7	581.1	582.6	579.5	581.0	581.1	579.3	578.0	580.7	582.7	585.3	581.6	580.3	581.2	583.5	584.[illegible]
35	582.4	581.1	583.5	585.4	583.4	580.8	582.2	584.5	583.0	582.4	587.1	587.9	586.8	586.6	584.7	589.4	587.4	587.[illegible]
30	587.9	586.7	587.3	587.3	585.6	584.8	585.6	587.0	585.6	585.1	589.9	589.9	588.7	588.6	588.4	589.4	590.0	589.[illegible]
25	586.9	586.9	587.7	588.1	588.0	587.4	587.6	587.6	586.7	586.5	589.0	589.7	589.5	588.8	589.8	590.6	590.9	590.[illegible]
20	586.8	587.9	587.6	588.1	588.7	588.4	588.1	587.2	586.6	587.0	588.0	588.9	589.4	588.3	589.2	590.3	590.7	590.[illegible]

MEAN MONTHLY HEIGHT FIELD 1957 273 500 S.H. FIG. 23

LAT \ LONG	0	10	20	30	40	50	60	70	80	90	100	110	120	130	140	150	160	170
90	486.0	486.0	486.0	486.0	486.0	486.0	486.0	486.0	486.0	486.0	486.0	486.0	486.0	486.0	486.0	486.0	486.0	486.0
85	487.6	487.1	487.0	487.2	487.6	488.8	489.5	490.5	491.2	491.9	492.1	491.9	491.1	490.2	489.0	487.6	486.4	485.0
80	488.4	487.5	487.2	487.6	488.8	490.8	492.2	494.2	495.7	497.0	497.4	497.0	495.5	493.7	491.2	488.5	486.1	483.3
75	489.8	487.3	486.3	487.0	488.6	490.0	491.7	493.9	496.7	499.5	500.5	500.1	498.0	496.2	493.3	489.9	486.6	483.1
70	493.2	489.4	488.3	489.2	490.1	489.9	489.1	489.4	491.3	494.4	496.7	497.4	497.6	497.3	496.0	494.3	492.0	489.5
65	500.1	496.9	496.0	496.2	496.0	494.5	491.7	489.2	488.9	489.7	491.8	492.9	497.4	501.4	502.9	503.7	503.8	503.8
60	511.0	508.3	507.7	506.4	505.6	502.7	499.1	496.4	494.4	493.5	495.1	498.8	505.3	509.9	512.7	515.2	518.3	520.9
55	522.4	520.7	519.4	518.5	517.6	515.0	509.8	508.0	508.2	507.3	508.5	513.3	518.1	522.3	525.6	529.2	534.0	537.1
50	534.3	533.7	532.3	532.0	531.8	529.6	525.7	524.7	525.4	524.4	525.9	529.1	531.3	534.2	536.6	540.4	545.2	548.6
45	546.4	546.1	545.1	546.4	547.8	547.1	544.8	544.1	542.8	541.8	542.6	543.8	543.9	544.8	546.4	548.1	551.4	555.4
40	558.2	557.6	557.0	559.7	562.1	562.7	563.2	562.0	558.6	556.5	556.0	556.2	555.4	555.7	554.5	554.4	554.7	558.0
35	568.8	567.9	568.2	571.0	573.4	574.3	575.1	575.5	570.6	568.1	567.3	566.4	566.1	565.6	563.2	561.5	559.2	561.1
30	577.1	576.2	577.6	581.2	582.1	581.5	581.4	580.7	578.9	577.0	576.1	574.8	574.4	573.4	570.6	569.1	566.6	567.1
25	583.6	582.5	584.7	587.2	586.3	584.5	584.8	584.8	584.1	582.6	581.0	580.5	580.2	580.8	576.9	575.4	574.5	575.4
20	587.3	586.6	587.8	588.1	587.4	586.3	586.6	587.4	587.0	586.4	585.4	584.2	583.1	584.2	581.0	580.2	580.8	582.6

MEAN MONTHLY HEIGHT FIELD 1957 273 500 S.H.

LAT \ LONG	180	170	160	150	140	130	120	110	100	90	80	70	60	50	40	30	20	10
90	486.0	486.0	486.0	486.0	486.0	486.0	486.0	486.0	486.0	486.0	486.0	486.0	486.0	486.0	486.0	486.0	486.0	486.0
85	484.1	484.0	483.9	483.9	483.9	484.3	485.4	486.7	488.0	489.1	489.8	490.6	491.0	491.1	490.7	490.8	489.1	488.1
80	481.5	481.3	481.8	481.0	481.1	481.9	484.0	486.6	489.8	491.4	492.9	494.4	495.3	495.5	494.6	493.2	491.4	489.5
75	481.0	479.7	479.3	479.6	480.7	482.6	485.8	489.4	492.3	495.1	497.1	498.8	500.5	501.2	500.8	498.6	496.3	493.0
70	487.8	485.9	485.0	486.8	489.4	493.0	496.3	498.9	500.6	500.6	500.6	502.1	504.4	506.1	506.6	505.2	502.3	497.7
65	503.9	503.1	503.2	504.5	506.6	508.6	510.4	511.7	511.3	509.7	507.4	508.4	510.3	512.7	513.8	513.2	510.4	505.7
60	522.2	522.2	522.2	522.5	523.6	524.2	524.1	523.9	522.8	520.3	517.4	516.6	517.9	520.1	521.6	522.2	519.7	515.8
55	538.2	538.3	538.0	537.9	538.2	537.1	535.7	534.9	533.3	531.7	528.6	527.8	527.7	529.5	530.2	531.0	529.6	526.3
50	549.4	549.8	549.7	550.2	549.2	547.9	546.2	544.7	544.5	544.2	541.3	539.1	538.6	540.1	540.6	540.6	539.4	536.5
45	555.8	556.8	557.7	558.8	558.1	556.1	554.5	553.7	555.8	555.7	552.7	549.5	549.6	551.0	551.2	550.0	549.4	547.4
40	559.7	560.9	562.8	564.4	564.1	562.1	561.0	562.6	565.4	566.0	562.7	559.4	558.4	559.7	560.0	559.3	559.1	558.2
35	563.4	565.5	567.4	568.1	567.8	567.1	567.7	570.5	573.6	573.6	570.1	568.2	567.1	566.2	566.3	567.2	568.3	568.6
30	569.1	571.1	572.3	572.1	572.8	572.5	574.9	577.4	580.1	579.3	576.4	574.7	573.1	572.7	572.7	573.5	576.8	577.0
25	577.2	578.3	577.8	576.9	576.9	577.9	580.2	582.3	584.1	583.4	581.7	580.5	579.6	579.2	579.2	580.1	582.3	583.6
20	584.3	584.0	582.9	581.7	581.6	582.2	584.0	586.4	587.5	586.7	585.3	584.7	584.0	584.0	584.1	585.8	586.7	587.5

FIG. 22 — NORTHERN HEMISPHERE
FIG. 23 — SOUTHERN HEMISPHERE

MONTHLY MEAN GEOPOTENTIAL HEIGHT VALUES, 500 mb SEPTEMBER 1957 UNITS — DEKAMETERS

To obtain a more realistic picture, the same data were transcribed on a polar stereographic map. The resulting contours are shown in Figures 24 and 25.

The monthly mean contours in the northern hemisphere depict a configuration of about hemispheric wave number five. Starting from Greenwich meridian going eastward, the first major trough line seems to be oriented in north-south direction in Central Europe followed by a less pronounced trough somewhere in the sector of 80E to 90E. Other major troughs that successively followed were (i) the one in the eastern Siberian region down to Korea, (ii) the one at the western coast of Alaska with the axis slightly tilted towards west in the middle section, and (iii) the last one in the Hudson Bay area stretching downward as far as the southeastern United States. A characteristic pattern of mean maps is a trough in the land area and a ridge in the ocean and this is noticeably manifested here.

The southern hemisphere contour structure shows tighter gradient, smoother waves manifested by less pronounced troughs and ridges. There is a closed contour centered at Ross Sea (75S, 155E). The relative predominance of water surfaces over land areas tends to smooth out the contours because the differential heating in the surface does not produce strong thermal differences in the upper layers of the atmosphere.

Zonally-averaged Mean Flow and Perturbation Patterns in Both Hemispheres

To break down the monthly mean contours into their zonally-averaged mean flow and perturbations, and for a better resolution of the latter and their consequential display in pure form, the mean height for each latitude circle was computed. These latitudinally-averaged values form the basis of parallel contours in the direction of zonal flow which serve to represent the zonal mean flow of the whole atmospheric system at 500 mb. Then the deviations or anomalies of each grid point mean

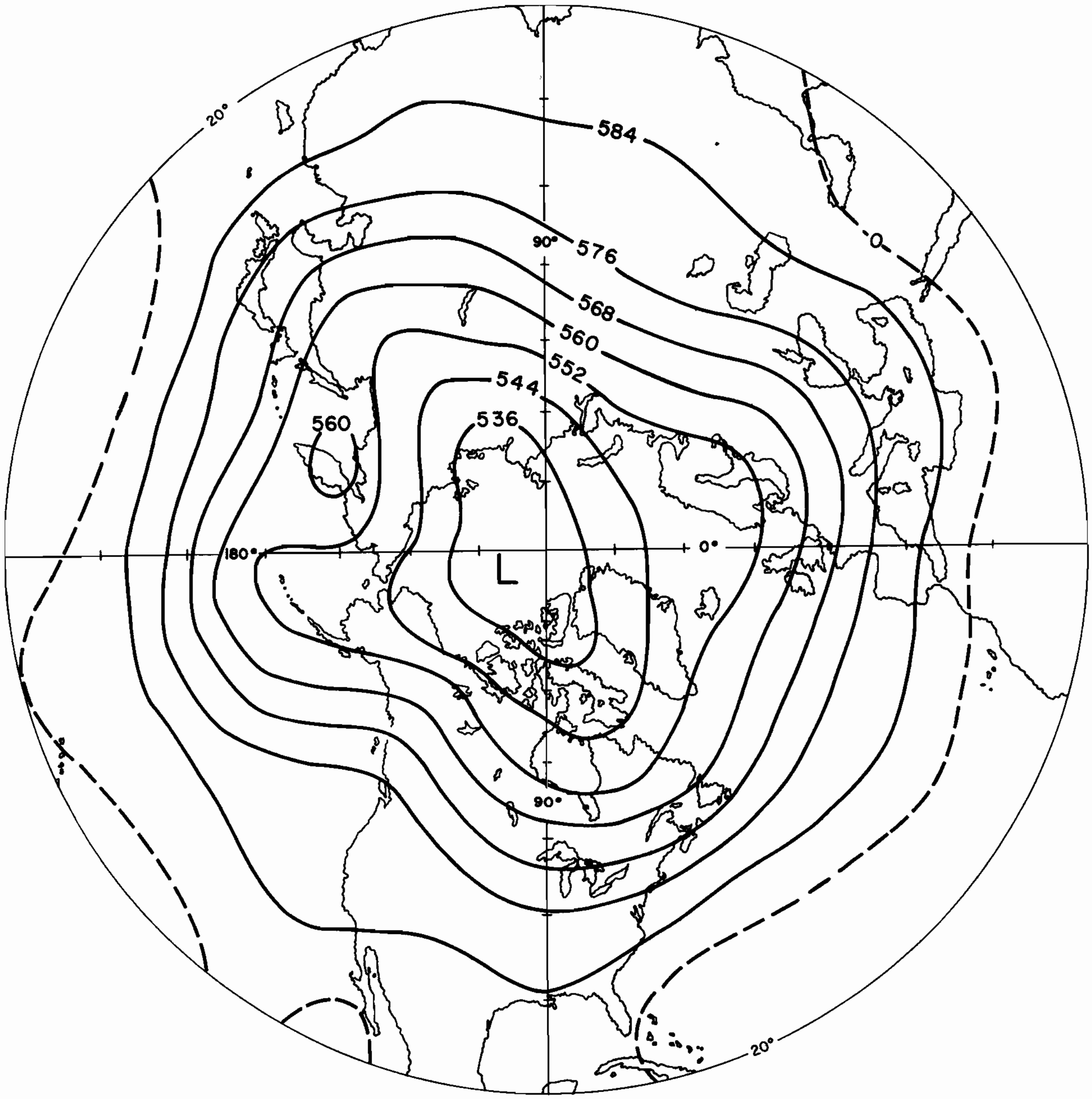

FIGURE 24. MONTHLY MEAN GEOPOTENTIAL HEIGHT FIELD, 500 MB
NORTHERN HEMISPHERE, SEPTEMBER, 1957.

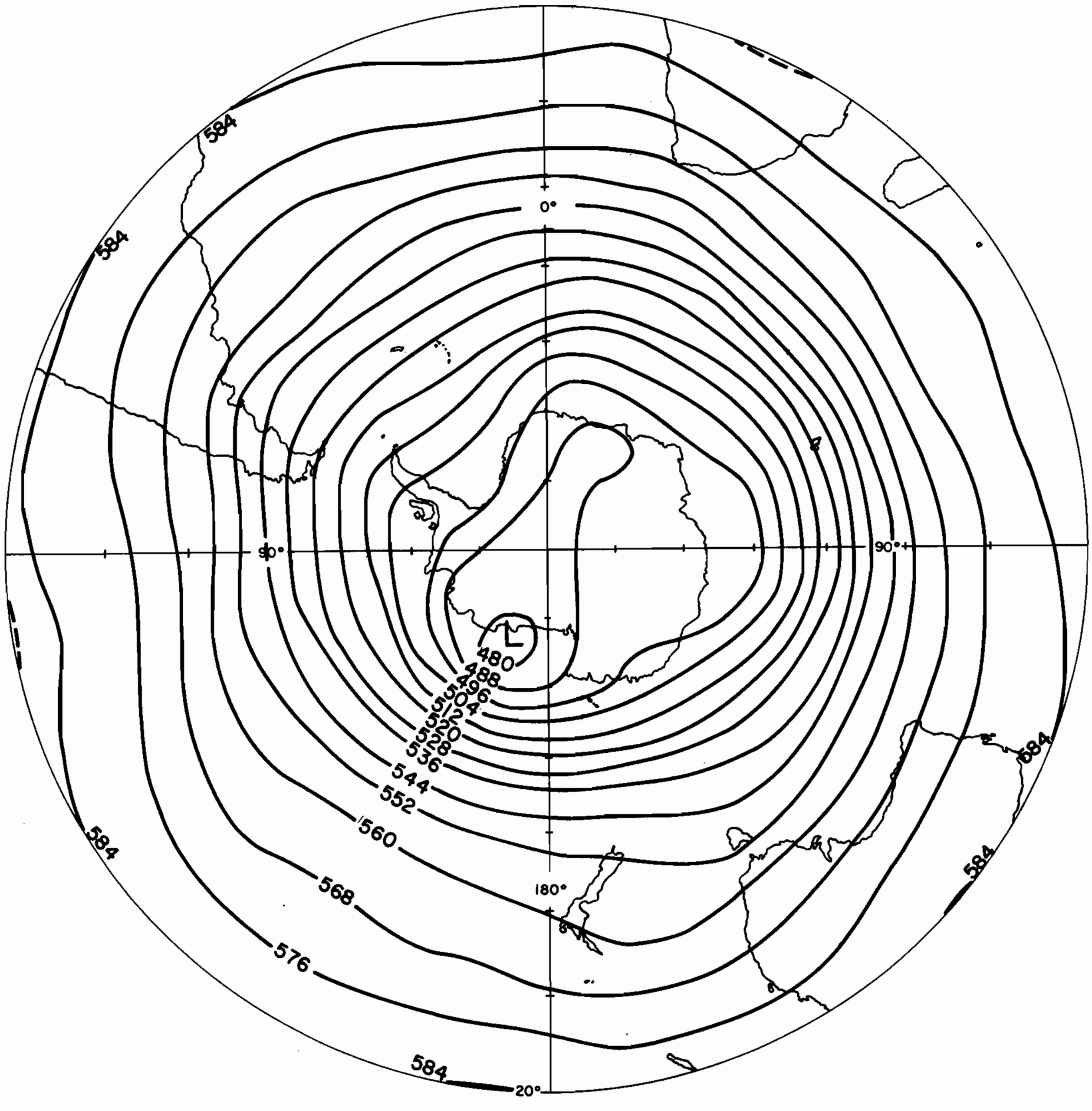

FIGURE 25. MONTHLY MEAN GEOPOTENTIAL HEIGHT FIELD, 500 MB
SOUTHERN HEMISPHERE, SEPTEMBER, 1957.

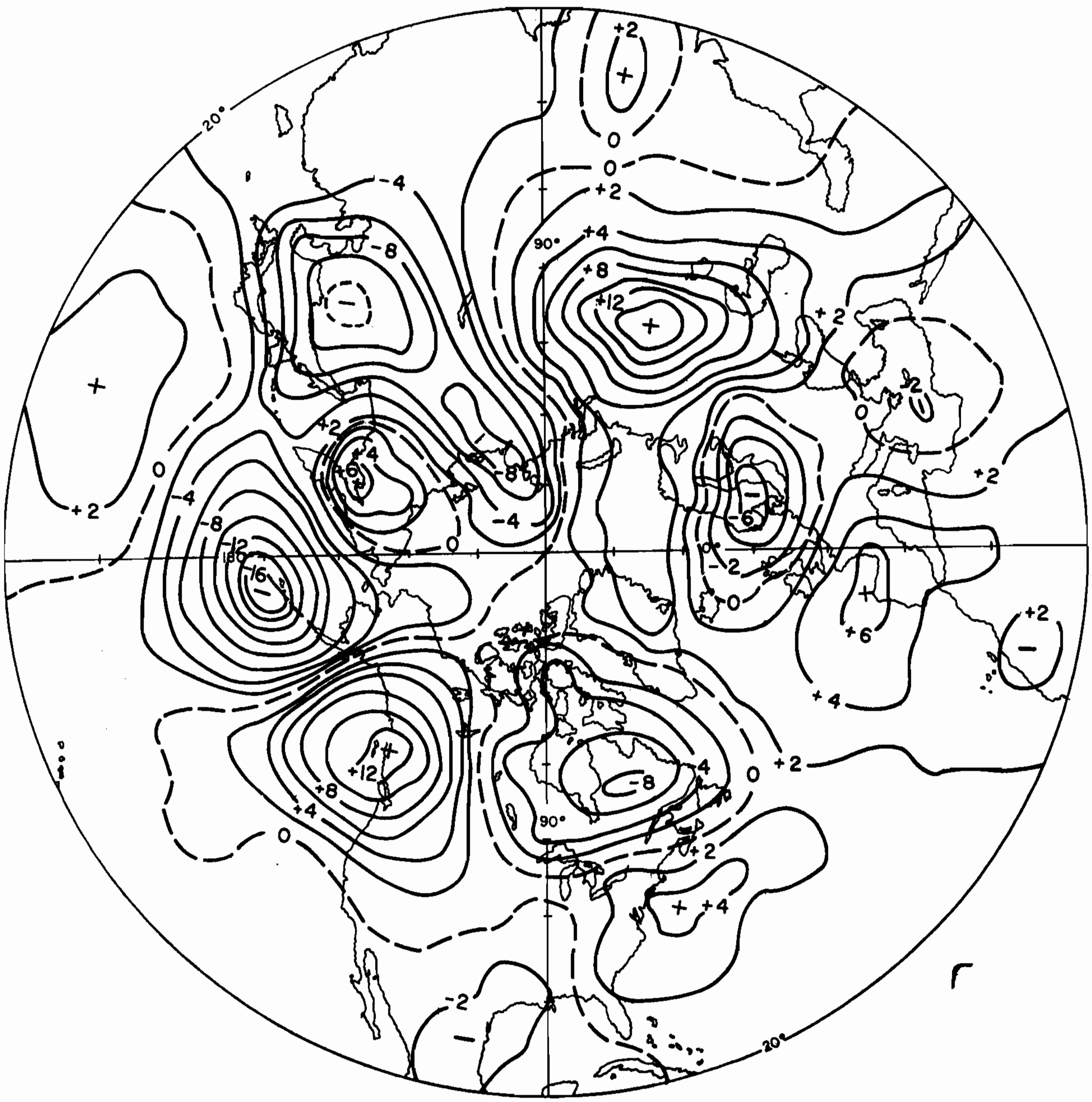

FIGURE 26. PURE PERTURBATIONS OF THE MONTHLY MEAN 500 MB

NORTHERN HEMISPHERE, SEPTEMBER, 1957.

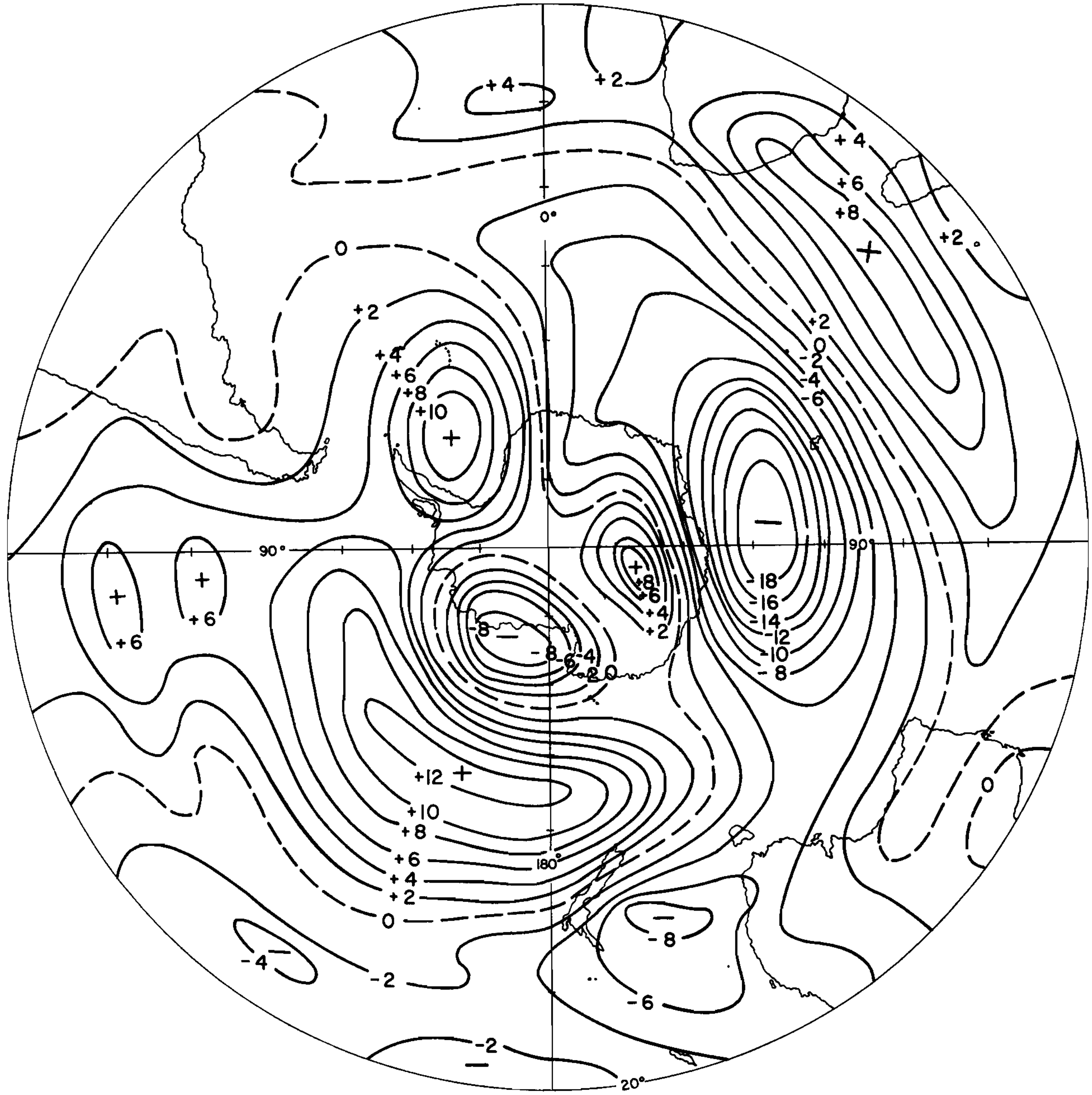

FIGURE 27. PURE PERTURBATIONS OF THE MONTHLY MEAN, 500 MB SOUTHERN HEMISPHERE, SEPTEMBER, 1957.

height value from the zonally-averaged values were computed and entered at all grid points. Isopleths of equal deviations were drawn with spacings of two dekameters. These represent the perturbations embedded in the mean flow. It is seen that the perturbations come out more prominently when depicted in this manner.

In Figure 26 which shows the perturbations in the northern hemisphere, the alternating centers of maximum positive and negative deviations lie mostly in the belt of 40N-60N. This observation tallies closely with the confirmed existence of cyclonic disturbances in this latitudinal sector.

The other centers of less pronounced deviations are located in the low latitudes (20-30 degrees) at longitudes 160E and 90W.

The centers of maximum positive deviations lie in axes corresponding to the ridges and the centers of maximum negative deviations in axes corresponding to the troughs. This corroborates the findings that were deduced earlier from the monthly mean maps. Prominent lines of zero deviations should provide a good measure of the distinctive hemispheric wave number of the perturbation pattern.

Again, these deviations were plotted on polar stereographic maps for better analysis and more realistic perspective.

In the southern hemisphere, the zonal parallel contours have tighter gradient as compared with the northern hemisphere. This result was expected in view of the previous quantitative measurements of the zonal flow energy described earlier in this paper which showed larger amounts in the southern hemisphere. Likewise, the isolines of deviations have tighter gradients in the southern hemisphere, although the number of maxima and minima is considerably less than in the northern hemisphere. The locations of these cells are found in mid-latitudes. It is also significant that the maximum values for the southern hemisphere are at smaller wave numbers than those for the northern hemisphere.

SUMMARY AND CONCLUSIONS

In the extensive computations of the atmospheric energy at 500 mb as a function of zonal wave numbers, Fourier series analysis was the basic technique employed to compute the zonal and meridional components of kinetic energy. Variations of geopotential height with latitude (ϕ) and longitude (λ), and geostrophic wind approximations constituted the main mathematical postulates embodied in the entire energy computations for both hemispheres.

Profiles were drawn to depict the significant variations of either the zonal or perturbation energy with time, latitude, and zonal wave numbers. Monthly mean values were also obtained to isolate the standing waves from the moving or transient waves.

Attempts were made to associate the most essential aspects of the energy variation and distribution with temporary and semi-permanent synoptic features and geographical characteristics.

Equally important with the various energy spectra analyses as functions of different pertinent parameters was the over-all relative comparison of the energy measurements between the two hemispheres, taking into consideration the disparity in season (September is late summer in northern hemisphere and late winter in southern hemisphere) and their widely different water and land distributions.

Based initially from the raw data extracted from the hemispheric International Geophysical Year World Weather Daily 500 mb charts for the full month of September 1957, the following conclusions were arrived at:

(i) The eddy or perturbation energy in both hemispheres are remarkably of the same magnitude (1.35×10^{14} kilojoules mb^{-1}), and the spread along the zonal wave numbers are not greatly different from one another.

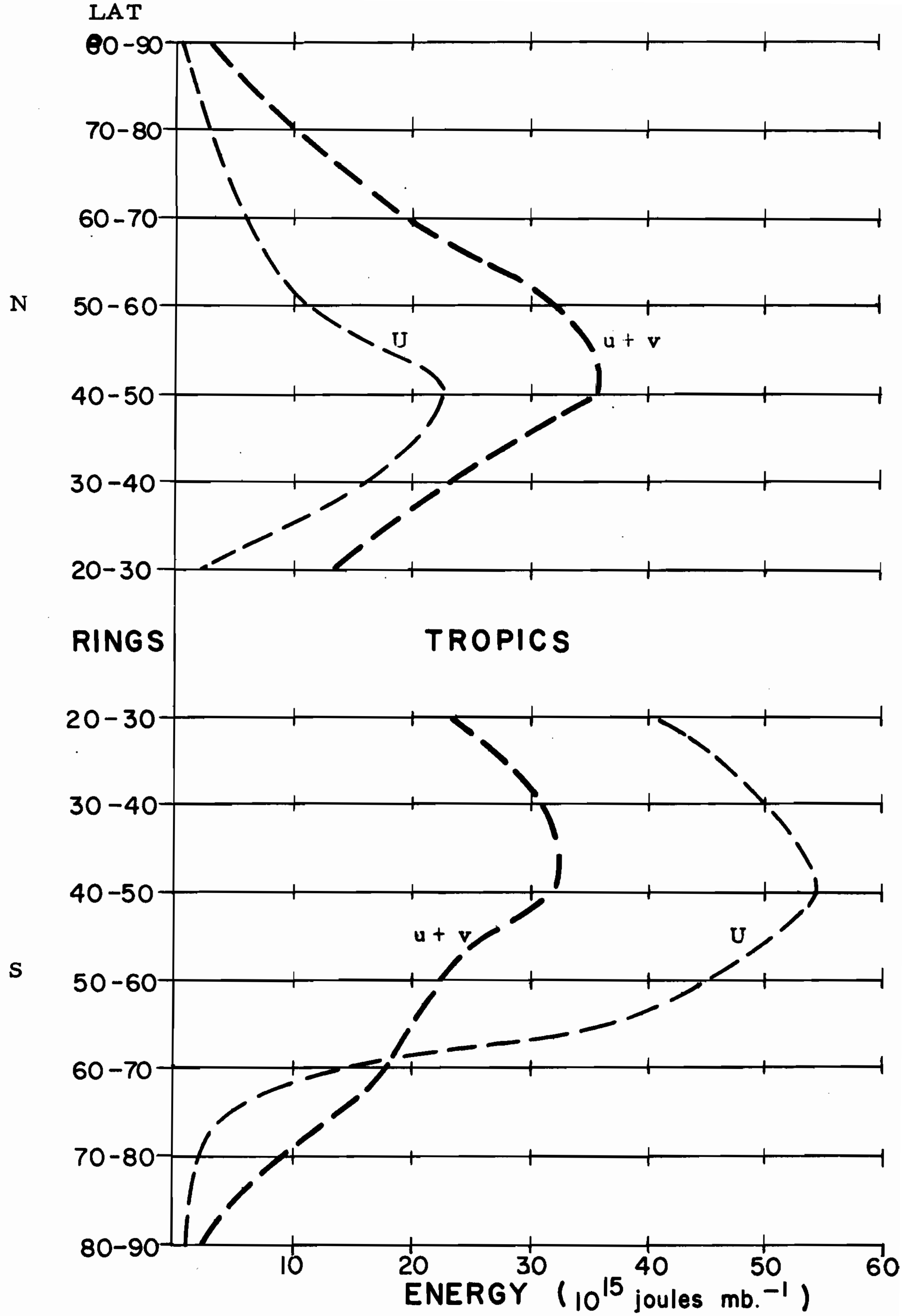

Figure 28. Geostrophic kinetic energy profiles in both hemispheres, 500 mb, September, 1957.

(ii) The zonal flow energy in the southern hemisphere is roughly three times that of the northern hemisphere. The differences in land-sea surface distribution, rather than changes in season, are likely the major factors in this inequality.

(iii) In both hemispheres, the maximum values of energy are concentrated in the latitudinal rings of 40-50 degrees and 50-60 degrees. This holds true for both zonal flow and perturbation energies. Strong westerlies in this belt and frequent occurrence of transient cyclones in this sector support the above findings.

(iv) Wave numbers 1 and 2 in the southern hemisphere and wave numbers 2 and 4 in the northern hemisphere have the greatest share of the perturbation energy. Wave numbers higher than 10 have negligible amounts of energy.

(v) In the spectra of mean perturbation energy as a function of wave numbers in both hemispheres, the u components are greater than the v components in the long, quasi-stationary waves (1 to 3) and vice versa in the rest of the other significant waves.

(vi) The energy of standing waves is concentrated in wave number 4 about the middle latitudes in the northern hemisphere, and at wave numbers 1 and 2 at rings 40S - 50S and 60S - 70S in the southern hemisphere.

(vii) The pattern of the distribution of the moving or transient wave energy is quite similar to that of the total kinetic energy in both hemispheres.

STATUS OF THE PROBLEM AND SUGGESTIONS FOR FURTHER WORK

The results that emerged from this limited investigation should be of interest to those considering an exhaustive study of the energetics of the atmosphere.

The scheme of a more thorough study should embrace both time and space expansion, i.e., if possible, a whole year of hemispherical data for both hemispheres and at various constant pressure strata of both troposphere and stratosphere.

The interactions, conversions, and exchange phases of energy should be probed in all their aspects to correlate with the findings regarding distribution and concentration of energy.

The investigation of the tropical zone to complete the global picture should also be included for closer tie-ups between the two hemispheres. In this connection, the writer regrets that he was not able to include the tropics in his study because the I.G.Y. World Weather Daily Maps, Part II (25S - 25N), had height contours instead of streamlines and isotachs, thus negating the feasibility of extracting directly the magnitude of the wind components at each grid point. Also, the inapplicability of the geostrophic approximations does not encourage very much the inclusion of the tropical data in the basic layout of the preparation program for this paper.

The advent of modern automatic, telemetering devices that probe the atmosphere and its outlying space complex should really pave the way for a more precise understanding of our enveloping atmosphere. The high-speed computing machines have apparently gone a long way in the solution of a major problem in meteorological research, that of extensive computations of fairly complicated problem formulae.

A remote aim of this study is to correlate the distribution and concentration of energy with our common knowledge of the definite sectors in our oceans which are perennial breeding grounds of our typhoons and hurricanes at certain months of the year. An enterprising researcher in the near future might come up with something significant if he follows this lead.

So far, energy budget researches done in relation to typhoon or hurricane activity are mostly local in scale, the writer is not aware of anyone involved in a study of energy problems, connected with these intense cyclonic circulations, on a global or planetary scale.

ACKNOWLEDGEMENTS

The writer is grateful to Professor B. W. Boville for advice, encouragement, and stimulating discussion.

Acknowledgement is made to Messrs. B. V. Cabacungan and J. de las Alas for their extensive help in extracting data from the I. G. Y. World Weather Maps; to Mr. H. L. Steinberg for writing much of the computer program; to Miss Lise Filion for punching computer cards; to Mrs. H. B. Kruczkowska for drafting diagrams; and to Mrs. S. MacKinnon for preparing the typescript.

Acknowledgement is also made to staff of the McGill Computing Centre for their help and advice in programming, and for the use of the IBM 7040, 32,000-word digital computer.

The writer wishes to extend his deepest appreciation to the External Aid Office of the Canadian government for the award of a scholarship at McGill University under the auspices of the Colombo Plan, and to his own government - of the Republic of the Philippines - for giving him the opportunity to avail himself of such a privilege.

REFERENCES

Barrett, E. W., 1958: "Some applications of harmonic analysis to the study of the general circulation", Univ. of Chicago, Dept. of Meteorology (Doct. thesis), 204.

Bolin, B., 1950: "On the influence of the earth's orography on the general character of the westerlies", Tellus, 2, 184-195.

Boville, B. W., and M. Kwizak, 1959: "Fourier analysis applied to hemispheric waves of the atmosphere", Meteorological Branch, Canada, TEC-292.

Boville, B. W., 1961: "A dynamical study of the 1958-59 stratospheric polar vortex", Pub. in Met. No. 36, Arctic Met. Research Group, McGill University, 134 p.

Charney, J. G., 1947: "The dynamics of long waves in a baroclinic westerly current", J. Meteor., 4, 135-162.

Eady, E. T., 1949: "Long waves and cyclone waves", Tellus, I, 3, 33-52.

Eliasen, E., 1958: "A study of the long hemispheric waves on the basis of zonal harmonic analysis", Tellus, 10, 206-215.

Godson, W. L., 1959: "The application of Fourier analysis to meteorological data", Meteorological Branch, Canada, TEC-295.

Graham, R. D., 1955: "An empirical study of planetary waves by means of harmonic analysis", J. Meteor., 12, 298-307.

Haltiner, J. G. and F. L. Martin, 1957: "The general circulation", Dynamical and Physical Meteorology, 415-453.

Hare, F. K., 1962: "Recent developments in dynamic and synoptic climatology". (Paper read at Asheville, October 23, 1962, Conference on Climatology, American Meteorological Society.)

Nielsen, A. W., 1959: "A study of energy conversion and meridional circulations for the large-scale motion in the atmosphere", Monthly Weather Review, 87, 319-332.

Obasi, G.P., 1963: "Atmospheric momentum and energy calculations for the southern hemisphere during the I.G.Y.", Scientific Report, No. 6, Planetary Circulations Project, Dept. of Meteorology, Mass. Inst. of Tech.

Pisharoty, P.R., 1954: "The kinetic energy of the atmosphere", Investigations of the General Circulation of the Atmosphere, Final Report No. AF 19(122)-48, General Circulation Project, Dept. of Meteorology, Univ. of California.

Saltzman, B., 1957: "Equations governing the energetics of the larger scales of atmospheric turbulence in the domain of wave number", J. Meteor., 14, 513-523.

Saltzman, B., 1958: "Some hemispheric spectral statistics", J. Meteor., 15, 259-263.

Saltzman, B. and A. Fleisher 1959: "The exchange of kinetic energy among larger scales of atmospheric motion", Studies of the Atmospheric General Circulation III, Final Report, Mass. Inst. of Tech., 28-34.

Starr, V.P., 1948: "An essay on the general circulation of the atmosphere", J. Meteor., 5, 39-43.

Starr, V.P., 1953: "Note concerning the nature of large scale eddies in the atmosphere", Tellus, 5, 494-498.

Van Mieghem, J., 1960: "Zonal harmonic analysis of the northern hemisphere geostrophic wind field", Monograph No. 8, International Union of Geodesy and Geophysics.

White, R.M. and Cooley, D.S., 1956: "Kinetic energy spectrum of meridional motion in the mid-troposphere", J. Meteor., 13, 67-69.

REFERENCE CHARTS

I.G.Y. World Weather Maps, Part I, Northern Hemisphere, Sea Level and 500 mb Charts, issued by U.S. Dept. of Commerce, Sept. 1957.

I.G.Y. World Weather Maps, Part III, Southern Hemisphere, Sea Level and 500 mb Charts, issued Republic of South Africa, Sept. 1957.

Daily 100 mb and 50 mb and Three Times Monthly 30 mb Synoptic Weather Maps of the I. G. Y. Period, U.S. Dept. of Commerce, Sept. 1957.

Daily Aerological Cross Sections, Pole to Pole Along Meridian 75°West for the I. G. Y. Period, U. S. Dept. of Commerce, Sept. 1957.

Normal 500 mb Charts for the Northern Hemisphere; Annual, seasonal, and monthly with monthly standard deviations, U.S. Navy Weather Research Facility, Sept. 1957.

Charney, J.G., 1951: "Dynamic forecasting by numerical process", Compendium of Meteor., 470-482.

APPENDIX

TABLES I.- IV

TABLE I. Monthly Mean Perturbation Energy for Northern Hemisphere, September 1-30, 1957. Units, 10^{14} joules mb^{-1}.

Zones / Wave No.	(1) 20°-40°		(2) 40°-60°		(3) 60°-80°		(4) 20°-90°	
	u	v	u	v	u	v	u	v
1	30.7	0.9	57.7	2.5	36.8	6.1	128.7	13.0
2	37.9	3.5	64.4	13.9	26.7	26.2	130.8	51.8
3	21.5	3.0	43.3	15.6	12.9	22.4	78.1	44.3
4	22.4	6.5	51.5	65.0	16.4	34.8	90.5	109.2
5	20.8	11.1	28.4	46.9	7.8	18.0	57.1	77.3
6	15.4	15.1	20.5	54.8	4.1	18.8	40.0	89.3
7	14.5	19.5	16.6	51.4	3.1	13.1	34.2	84.5
8	9.1	11.7	10.0	26.3	1.7	6.8	20.8	45.3
9	9.1	17.1	7.3	25.6	1.1	5.4	17.5	48.4
10	6.2	14.9	5.6	16.2	0.7	3.5	12.5	35.0
11	5.6	8.9	3.8	13.6	0.8	3.1	10.2	26.0
12	4.7	9.7	3.2	12.8	0.5	2.7	8.4	25.5
13	4.6	9.0	2.5	9.4	0.3	2.1	7.4	20.9
14	4.1	7.6	2.0	7.9	0.3	2.0	6.4	18.1
15	3.6	6.7	2.3	8.2	0.3	2.0	6.2	17.5
Totals	210.2	145.2	320.1	370.1	113.5	167.0	648.8	706.0

TABLE II. Monthly Mean Perturbation Energy for Southern Hemisphere, September 1-30, 1957. Units, 10^{14} joules mb^{-1}.

Zones / Wave No.	(1) 20°-40° u	(1) 20°-40° v	(2) 40°-60° u	(2) 40°-60° v	(3) 60°-80° u	(3) 60°-80° v	(4) 20°-90° u	(4) 20°-90° v
1	52.2	1.9	82.5	8.1	44.8	9.6	182.2	22.3
2	47.2	8.4	53.7	13.0	38.9	29.1	141.6	57.9
3	32.3	7.4	31.2	24.4	13.4	30.1	77.1	63.3
4	39.9	16.2	27.2	60.8	10.6	28.9	77.8	106.8
5	31.5	30.3	23.7	47.4	5.2	15.3	60.4	93.5
6	19.4	30.6	9.9	30.2	2.6	9.5	31.9	70.7
7	20.4	39.5	10.1	27.1	1.9	5.6	32.4	72.4
8	11.1	26.0	6.4	21.9	0.9	3.5	18.4	51.6
9	10.5	23.8	5.1	18.9	0.8	3.2	16.4	46.1
10	7.1	15.2	3.0	11.0	0.4	2.0	10.5	28.4
11	5.0	12.3	2.3	8.6	0.3	1.6	7.6	22.7
12	4.2	11.1	1.4	6.1	0.2	1.5	5.8	18.9
13	4.2	11.4	1.2	4.6	0.2	1.5	5.6	17.8
14	2.5	7.1	1.1	4.3	0.2	1.0	3.8	12.7
15	2.7	7.1	0.9	3.7	0.2	1.4	3.8	12.5
Totals	290.2	248.3	259.7	290.1	120.6	143.8	675.3	697.6

TABLE III. Energy of the standing waves as differentiated from the total kinetic energy for both hemispheres. Units, 10^{14} joules mb^{-1}.

Wave Number	N. Hemisphere Total K. E.	N. Hemisphere K. E. of the Mean	S. Hemisphere Total K. E.	S. Hemisphere K. E. of the Mean
1	141.7	45.9	204.5	135.2
2	181.6	51.3	199.5	95.3
3	122.2	28.5	140.4	8.1
4	199.6	65.2	184.6	10.4
5	134.4	22.0	154.0	16.4
6	129.4	17.4	102.6	2.6
7	118.6	12.9	104.8	6.0
8	66.2	2.2	70.0	3.3
9	65.8	6.7	62.5	1.7
10	47.4	3.9	39.0	1.1
11	36.2	2.7	30.3	1.8
12	34.0	1.4	29.7	0.9
13	28.4	3.7	23.5	0.8
14	24.5	1.5	16.4	0.7
15	23.7	1.2	16.2	0.9

TABLE IV. Latitudinal Ring Energy Values. (10^{14} joules mb^{-1})

Ring Central Latitude	Zonal Mean Flow S.H.	Zonal Mean Flow N.H.	Perturbation S.H.	Perturbation N.H.
25	402.7	23.0	225.8	133.0
35	494.4	167.7	313.1	223.6
45	544.4	236.5	326.7	361.1
55	451.0	98.4	223.4	328.5
65	167.1	55.2	181.5	182.5
75	11.4	31.2	82.9	97.5
85	3.6	5.7	20.1	28.6
Totals	2074.5	636.2	1354.8	1372.9